Research Paper

THEMED ISSUE: Seismotectonics of the San Andreas Fault System in the San Gorgonio Pass Region

GEOSPHERE

GEOSPHERE, v. 16, no. 4

https://doi.org/10.1130/GES02121.1

11 figures; 1 table; 1 set of supplemental files

CORRESPONDENCE: cwill13@vt.edu

CITATION: Cochran, W.J., Spotila, J.A., and Prince, P.S., 2020, Incipient evolution of the Eastern California shear zone through the transpressional zone of the San Bernardino Mountains and San Gorgonio Pass, California: Geosphere, v. 16, no. 4, p. 919–935, https://doi.org/10.1130/GES02121.1.

Science Editor: Andrea Hampel
Guest Associate Editor: Doug Yule

Received 10 February 2019
Revision received 22 March 2020
Accepted 28 April 2020

Published online 5 June 2020

Incipient evolution of the Eastern California shear zone through the transpressional zone of the San Bernardino Mountains and San Gorgonio Pass, California

William J. Cochran*, James A. Spotila*, and Philip S. Prince*

Department of Geosciences, Virginia Tech, 4044 Derring Hall, Blacksburg, Virginia 24061, USA

ABSTRACT

The nature of the connection between the Eastern California shear zone (ECSZ) and the San Andreas fault (SAF) in southern California (western United States) is not well understood. Northwest of San Gorgonio Pass, strands of the ECSZ may be migrating south and west into the convergent zone of the San Bernardino Mountains (SBM) as it is advected to the southeast via the SAF. Using high-resolution topography and field mapping, this study aims to test whether diffuse faults within the SBM represent a nascent connection between the ECSZ and the SAF. Topographic resolution of ≤1 m was achieved using both lidar and unmanned aerial vehicle surveys along two Quaternary strike-slip faults. The Lone Valley fault enters the SBM from the north and may form an along-strike continuation of the Helendale fault. We find that its geomorphic expression is obscured where it crosses Quaternary alluvium, however, suggesting that it may have a low rate of yet-undetermined activity. The Lake Peak fault is located farther south and cuts through the high topography of the San Gorgonio massif and may merge with strands of the SAF system. We find that this fault clearly cuts Quaternary glacial deposits, although the magnitude of offset is difficult to assess. Based on our interpretation of geomorphic features, we propose that the Lake Peak fault has predominantly dextral or oblique-dextral motion, possibly with a slip rate that is comparable to the low rates observed along other strands of the ECSZ (i.e., ≤1 mm/yr). Comparing the geomorphic expressions of these faults is difficult, however, given that the erosive nature of the mountainous landscape in the SBM may obscure evidence of active faulting. Based on these observations, as well as the occurrence of other diffuse faults in the region, we suggest that dextral strain is overprinting the actively convergent zone of the SBM, thereby creating a throughgoing connection between the ECSZ and the SAF west of San Gorgonio Pass.

*E-mail: cwill13@vt.edu, spotila@vt.edu, psprince@vt.edu

INTRODUCTION

The transient evolution of continental transforms along obliquely deforming zones provides a window into the complexity of fault-strand development and crustal deformation (Cunningham and Mann, 2007). Complex fault patterns are commonly observed along nascent shear zones and are known to include conjugate fault sets, fault overprinting, and fault slip partitioning that results in dynamic rupture patterns (Harris and Day, 1993; Magistrale and Day, 1999; Rubin, 1996; Segall and Pollard, 1980). Along the southern San Andreas fault (SAF) system near San Gorgonio Pass in southern California (western United States), the activity, seismogenic role, and likelihood of throughgoing rupture of several major fault strands have been extensively debated (e.g., Kendrick et al., 2015; Morton and Matti, 1993; Yule, 2009; Yule and Sieh, 2003). A major complicating factor in this nexus of interacting faults is the potential influence of the Eastern California shear zone (ECSZ) (Fig. 1). Although many studies have focused on faults within the ECSZ to the north (Herbert et al., 2014; Oskin et al., 2007; Spinler et al., 2010; Thatcher et al., 2016), little work has been done assessing kinematics of potential connector faults located between the ECSZ and the SAF within the San Bernardino Mountains (SBM). Understanding the kinematics of these little-studied faults will provide insights on fault development in complex fault systems by helping to document how strain is transferred from the SAF to the ECSZ. In addition, characterizing these diffuse faults will contribute to understanding future earthquake sources in the heavily populated areas of southern California.

The complex connection between the ECSZ and the SAF in the vicinity of San Gorgonio Pass embodies three fundamental problems related to continental transform fault behavior. First, the possibility of a developing structural connection between the fault systems in the SBM relates to the problem of how discontinuous fault strands in shear zones integrate into throughgoing fault systems with progressive slip. Strike-slip faults are thought to lengthen and integrate by linking through gaps in faulting and become more linear with increasing deformation (Wesnousky, 1988). Yet this behavior is difficult to document, and faults may instead remain poorly integrated due to ongoing alteration and development of stepovers (i.e., slip strengthening) (Buscher and Spotila, 2007; Cowgill et al., 2004; Gomez et al., 2007). Second, the overlap between diffuse shear in the ECSZ and transpressional deformation along the SAF in the vicinity of the SBM illustrates how secondary deformation may evolve as neighboring crust is

advected along either side of a restraining double bend. Both sides of a strike-slip fault may move equally with respect to such a feature, but in some cases, it appears that propagation, or shunting, of adjacent, evolving transpressional or transtensional deformation fields may occur preferentially on one side of the double bend (Anderson, 1990; Burkett et al., 2016; Wakabayashi, 2007). Finally, the possibility that short, discontinuous structures play a role in accommodating deformation in the southernmost ECSZ may be relevant for understanding the discrepancy between geodetically and geologically determined slip rates (Blisniuk et al., 2010; Herbert et al., 2014; McGill et al., 2013, 2015; Oskin et al., 2008; Spinler et al., 2010; Spotila and Anderson, 2004; Thatcher et al., 2016). This discrepancy has been attributed to off-fault deformation along poorly constrained, short structures (Herbert et al., 2014; Shelef and Oskin, 2010), some of which were not even identified until they experienced historical rupture (Sieh et al., 1993). However, a complete kinematic picture of the ECSZ-SAF connection will not be acquired until all relevant, major structures have been adequately characterized.

The kinematics of slip transfer between the SAF and the southern ECSZ varies to the east and west of San Gorgonio Pass (Fig. 1). Some strands of the ECSZ appear to transfer slip indirectly to the south of their terminations at the Pinto Mountain fault into the domain of sinistral faulting and clockwise vertical-axis rotation in the eastern Transverse Ranges (Fig. 1) (Carter et al., 1987). Western strands of the southern ECSZ appear instead to terminate or propagate diffusely into the convergent zone of the SBM, which lies north of the restraining bend at San Gorgonio Pass (Figs. 1, 2) (Spotila and Anderson, 2004; Spotila and Sieh, 2000). Although short, discontinuous northwest-trending dextral faults have been mapped in the hanging wall to the thrust faults responsible for uplifting the SBM (Fig. 2), the degree to which these provide a throughgoing transfer system between the ECSZ and the SAF is unknown. These faults may merge with the Helendale, Old Woman Springs, and Johnson Valley faults to the north and the Mission Creek and Mill Creek faults and thrusts in San Gorgonio Pass to the south, thereby directly feeding slip from the restraining bend into the ECSZ (Fig. 2) (Kendrick et al., 2015; Matti and Morton, 1993; Yule and Sieh, 2003). However, little has been documented about the kinematics of these discontinuous dextral faults, and as a result, the kinematics of this fault confluence is not presently understood (Yule, 2009).

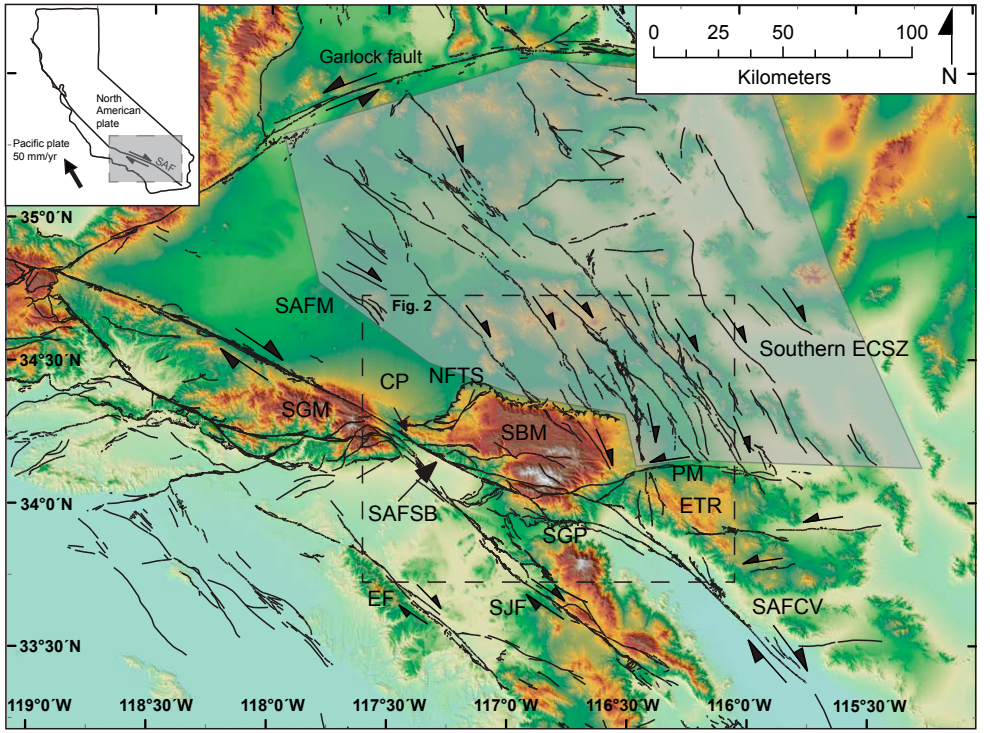

Figure 1. Fault map showing the relationship between the Eastern California shear zone (shaded) and the San Andreas fault zone, southern California. The base map is a digital elevation shaded relief hillshade product (with elevation overlain) from the ALOS Global Digital Surface Model (AW3D30) dataset with 1 arc second (i.e., 30 m) resolution. This dataset is publicly available at the OpenTopography website (www.opentopography.org). Inset: Location of San Andreas fault (SAF) and plate velocity vector from DeMets and Dixon (1999). CP—Cajon Pass; ECSZ—Eastern California shear zone; EF—Elsinore fault; ETR—eastern Transverse Ranges; NFTS—North Frontal thrust system; PM—Pinto Mountain fault; SAFCV—Coachella Valley segment of San Andreas fault; SAFM—Mojave segment of San Andreas fault; SAFSB—San Bernardino segment of San Andreas fault; SBM—San Bernardino Mountains; SGM—San Gabriel Mountains; SGP—San Gorgonio Pass; SJF—San Jacinto fault.

The purpose of this study is to test the plausibility of slip transfer from the SAF to the ECSZ via diffuse right-lateral faulting within the convergent SBM. Specifically, we use high-resolution topography and field mapping to assess the kinematics and evidence for recent activity along the Lake Peak and Lone Valley faults (Fig. 2). Prior mapping suggests that these faults displace previously mapped Quaternary surficial deposits (Dibblee, 1964b, 1967a, 1967b; Miller and Cossette, 2004), but displacement along these faults is unknown. We assess these faults in the context of whether they represent the southern penetration of the ECSZ into the SBM transpressional domain and evaluate what potential they have to contribute to slip transfer from the SAF to the ECSZ.

TECTONIC SETTING

San Andreas Fault

The SAF system south of the "big bend" consists of several major fault segments and strands, which decrease in slip rate southward as strain is transferred to other fault systems (Figs. 1, 2). The Mojave segment of the SAF accommodates ~35 mm/yr of dextral shear (Weldon and Sieh, 1985), which decreases to 25 mm/yr at Cajon Pass, where the San Bernardino strand and the San Jacinto fault diverge (Meisling and Weldon, 1989; Weldon and Sieh, 1985). Geologic slip rates of 8–15 mm/yr for the past 35 k.y. have been estimated for the San Bernardino strand (McGill et al., 2013). Studies suggest that the San Jacinto fault initiated between 2.4 and 1.0 Ma and has accommodated 1.3–1.8 cm/yr of slip during the Quaternary (Blisniuk et al., 2010; Onderdonk et al., 2015; McGill et al., 2015; Spinler et al., 2010). Both the SAF and San Jacinto fault south of Cajon Pass have been characterized by temporal and spatial variation in fault behavior, and the decrease in slip southward may in part be accommodated by a broad zone of distributed strain (Blisniuk et al., 2010; Matti and Morton, 1993).

The slip rate of the SAF decreases farther southward through San Gorgonio Pass to 14–17 mm/yr on the Coachella Valley segment (e.g., Behr et al., 2010). San Gorgonio Pass is a 20 km left step between the San Bernardino and Coachella Valley segments, along which no clear active, throughgoing dextral trace of the SAF exists. The stepover instead consists of a complex array of dextral strike-slip, reverse, and oblique-normal faults, which generate fault slip transfer, off-fault deformation, and rock uplift (Matti and Morton, 1993; Spotila et al., 2001; Yule and Sieh, 2003). The SAF through the pass has been modeled as rolling over with moderate (37°) northward dip to merge with the San Gorgonio Pass thrust zone (Fuis et al., 2012), which exhibits 4.2–8.4 mm/yr of dextral-oblique slip (Heermance and Yule, 2017) and ~2.5 mm/yr of reverse slip (Yule and Sieh, 2003). Modeling suggests that these faults may accommodate as much as 4.5 mm/yr of reverse slip (Cooke and Dair, 2011). The total strike-slip motion accommodated through San Gorgonio Pass has been estimated at ~6 mm/yr, or only one-third of the total slip coming northward from the Coachella Valley segment (Rangel and McGill, 2016). Both geodetic and numerical modeling suggests that the missing strain may be transferred north into the ECSZ (Loveless and Meade, 2011; McGill et al., 2013; Meade and Hager, 2005; Spinler et al., 2010), although the connectivity of the SAF through the pass has prompted suggestions of a possible barrier for rupture and therefore a strain accumulation zone (Yule, 2009; Yule and Sieh, 2003). South from San Gorgonio Pass, the Garnet Hill, Banning, and Mission Creek faults integrate into the Indio Hills fault, which constitutes the main strand of the SAF through the Coachella Valley (Behr et al., 2010; Gold et al., 2015).

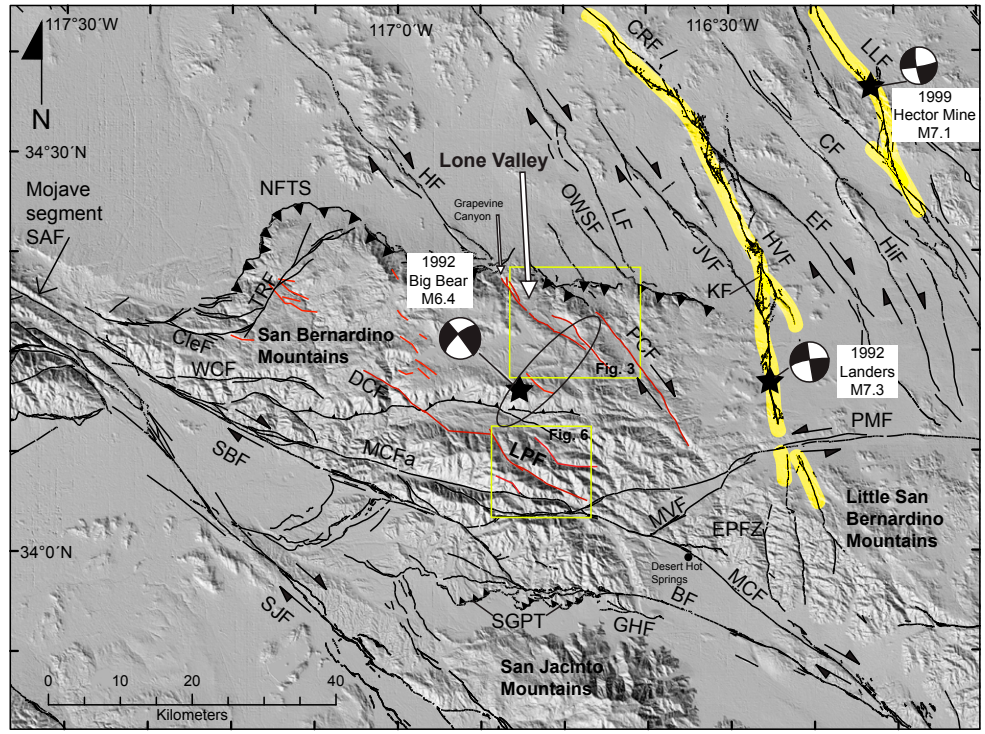

Figure 2. Fault map for the San Bernardino Mountains and southern Eastern California shear zone; faults are denoted in black and red. Black faults are from U.S. Geological Survey and California Geological Survey (2006); red faults were originally mapped by Dibblee (1964a, 1964b, 1967a, 1967b). Thick yellow lines represent surface rupture during the 1992 Landers earthquake (Sieh et al., 1993) and the 1999 Hector Mine earthquake (Hauksson et al., 2002). Black ellipse represents the rough trend of the epicentral location of the 1992 Big Bear aftershock sequence (Jones and Hough, 1995). The base map is a digital elevation shaded relief hillshade product from the ALOS Global Digital Surface Model (AW3D30) dataset with 1 arc second (i.e., 30 m) resolution. This dataset is publicly available at the OpenTopography website (www.opentopography.org). BF—Banning fault; CF—Calico fault; CleF—Cleghorn fault; CRF—Camp Rock fault; DCF—Deer Creek fault; EF—Emerson fault; EPFZ—Eureka Peak fault zone; GHF—Garnet Hill fault; HF—Helendale fault; HiF—Hidalgo fault; HVF—Homestead Valley fault; JVF—Johnson Valley fault; KF—Kickapoo fault; LF—Lenwood fault; LLF—Lavic Lake fault; LPF—Lake Peak fault; MCF—Mission Creek fault; MCFa—Mill Creek fault; MVF—Morongo Valley fault; NFTS—North Frontal thrust system; OWSF—Old Woman Springs fault; PCF—Pipes Creek fault; PMF—Pinto Mountain fault; SAF—San Andreas fault; SBF—San Bernardino fault; SGPT—San Gorgonio Pass thrust zone; SJF—San Jacinto fault; TRF—Tunnel Ridge fault; WCF—Waterman Canyon fault.

Eastern California Shear Zone

The ECSZ is a nearly 125-km-wide zone of diffuse dextral shear involving numerous northwest-striking faults that accommodate as much as 25% of the motion between the Pacific and North American plates (Dibblee, 1961; Dokka and Travis, 1990a, 1990b; Miller et al., 2001). The southern ECSZ in the Mojave Desert connects the SAF and extension in the Gulf of California with dextral shear and extension in the southwestern Basin and Range and Walker Lane (Plattner et al., 2010). Faults in the southern ECSZ have evolved diachronously since at least 4–6 Ma (Andrew and Walker, 2017; Glazner et al., 2002; Oskin and Iriondo, 2004; Oskin et al., 2007). Although individual faults exhibit only 1–10 km of right-lateral slip, the total dextral slip across the southern ECSZ is estimated at 50–75 km (Andrew and Walker, 2017; Dokka and Travis, 1990a; Glazner et al., 2002). In the southern Mojave Desert, the active ECSZ consists of six discontinuous, northwest-trending, 30- to 70-km-long dextral faults (i.e., Helendale, Lenwood, Camp Rock, Calico, Pisgah, and Ludlow faults) (Andrew and Walker, 2017; Oskin et al., 2008), which become more northerly oriented and bifurcate into numerous shorter fault segments southward toward the SAF (Fig. 2).

The SBM has several northwest-trending, high-angle faults that appear to connect with faults within the ECSZ (Fig. 2). To the southeast of the Helendale fault lies a northwest-trending fault within the graben-like Lone Valley. Although these faults lie along strike, previous mapping has not identified a direct, active connection between them through Grapevine Canyon (Dibblee, 1964a). Both sides of Lone Valley are topographically sharp and exhibit strong lineaments, suggesting two valley-bounding faults. We refer to these faults together as the Lone Valley fault (Fig. 3). Although the kinematics along these faults is unknown, Miller and Cossette (2004) suggested fault activity along the southwestern side of the valley during the Quaternary (Late Pleistocene to late Holocene). Along strike of the Lone Valley fault to the southeast lies the northwest-striking Pipes Canyon fault, where dextral offset is suggested by a channel deflection of ~1.8 km (Fig. 2). Northwest-trending faults

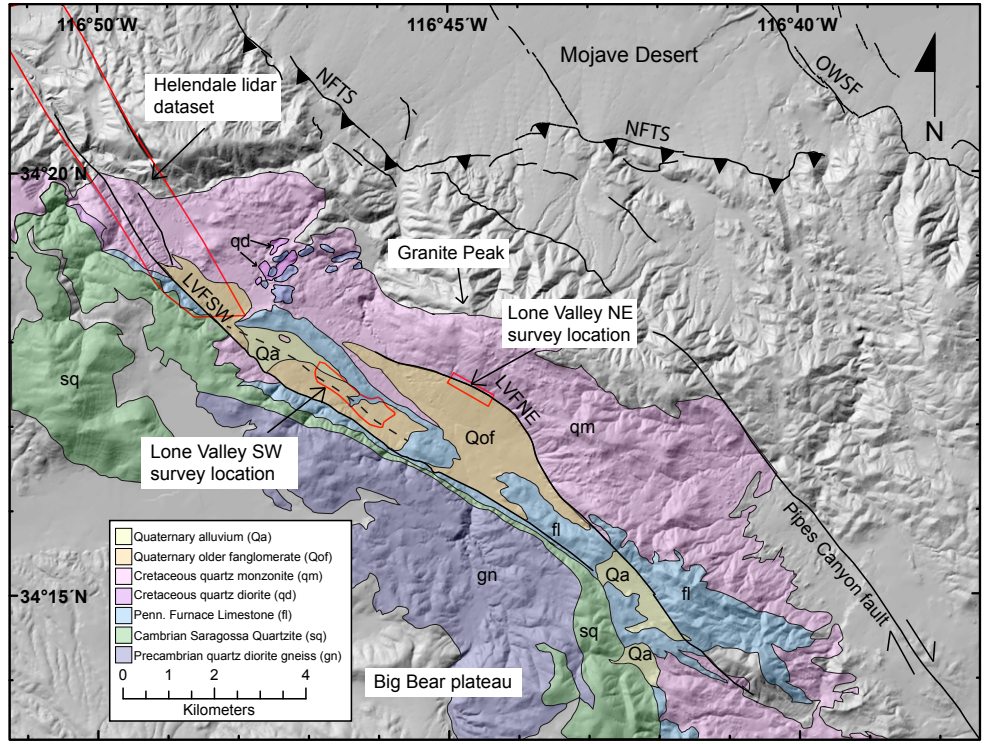

Figure 3. Fault location and bedrock geology map modified from Dibblee (1964a, 1964b, 1967a, 1967b) for Lone Valley. Further to the southeast, field reconnaissance was conducted on the Lone Valley fault and found that this section of the fault lacks geomorphic expression and was therefore not surveyed. Red outlines indicate data extent of high-resolution topography surveys (both lidar and unmanned aerial vehicle). The Helendale lidar survey data can be found at www.opentopography.org. Faults represented by black lines are from U.S. Geological Survey and California Geological Survey (2006). LVFNE—Lone Valley fault northeast; LVFSW—Lone Valley fault southwest; OWSF—Old Woman Springs fault; NFTS—North Frontal thrust system. Penn.—Pennsylvanian.

also occur within the core of the SBM, including the Lake Peak fault (previously referred to as the Dollar Lake fault by Spotila and Anderson [2004]) and the Deer Creek fault (Fig. 2). The Lake Peak fault, located within the North Fork Whitewater River drainage (Fig. 6), displaces Quaternary glacial deposits previously dated at 11–16 ka (Owen et al., 2003; Sharp et al., 1959). The Deer Creek fault occurs along strike to the northwest of, and may connect to, the Lake Peak fault (Dibblee, 1964b). The Deer Creek fault displays a prominent lineament that appears to offset a ridge, but other kinematic information is not available. There are also other short, northwest-striking faults throughout the SBM, but constraints on age, displacement, and rupture history are not known (Fig. 2). Nearly all of these faults cut through erosional, mountainous terrain, as opposed to depositional terrain similar to that hosting faults within the Mojave Desert, which could be an explanation as to why so little is understood about strike-slip faulting within the SBM.

It is not known whether these short, discontinuous high-angle faults represent southward penetration of the ECSZ into the transpressive SBM. Rock uplift of the SBM is a result of transpression along the SAF driven by convergence in

San Gorgonio Pass (Spotila and Sieh, 2000) (Fig. 2). In the northern SBM, convergence has been accommodated by motion along the south-dipping North Frontal thrust system and north-dipping Santa Ana thrust, defining the broad Big Bear block (Spotila and Sieh, 2000). In the south, convergence is accommodated on more steeply dipping structures, including strands of the SAF, and results in greater magnitudes of rock uplift (Spotila et al., 1998, 2001). Spotila and Anderson (2004) proposed a kinematic model in which the ECSZ penetrates the eastern portion of the Big Bear block, thereby terminating thrust faults to the east but permitting thrust faults to the west of the Helendale fault to remain active (Fig. 2). This model does not explain the potential existence of dextral faults in the central and western SBM, however, indicating the need for basic fault characterization of this region.

METHODS

Study Areas and Approach

We conducted neotectonic mapping and characterization in remote areas of the SBM to determine the activity of previously identified northwest-trending faults. Although bedrock maps have previously been constructed for these areas at coarse scales (e.g., 1:62,500; Dibblee, 1964b), a concerted neotectonic examination of the discontinuous faults of the central and eastern SBM has not been previously attempted. Because these faults occur in rugged terrain, we hypothesize that their neotectonic expression may be muted. The faults occur at high elevation, including across the >3-km-high San Gorgonio massif, and transect rugged hillslopes that presumably experience rapid erosion (Spotila and Sieh, 2000). In contrast, strands of the ECSZ to the north of the SBM have been characterized in well-preserved alluvial surfaces of the Mojave Desert. This difference in geomorphic terrain may translate to a preservational bias, in which faults in the SBM may have experienced more recent fault activity than would otherwise be interpreted based on coarse mapping and muted topographic expression.

We selected the Lake Peak and Lone Valley faults for further investigation, because they appeared most likely to display evidence for active faulting. We utilized high-resolution topography from both airborne lidar and aerial photogrammetry to characterize neotectonic activity of these faults. We also synthesized existing evidence for other dextral faulting within the SBM.

Data Collection

The airborne lidar survey encompassed a ~147 km² area along the Pinto Mountain, Mission Creek, Mill Creek, and Lake Peak faults, with a focus on the nexus of these converging strike-slip faults (Fig. 2). The survey was flown in 2016 by the National Center for Airborne Laser Mapping (NCALM; Houston, Texas, USA) using the three-channel Optech Titan Airborne Laser Terrain Mapper (channel 1: 1550 nm; channel 2: 1064 nm; channel 3: 532 nm). The scanner parameters affect the density of the laser pulses (Cochran, 2016). Four GPS ground stations were used for calculating the aircraft trajectory. The survey was performed during snow-off conditions to ensure that true topography was being returned from the laser sensor. A point density of 4.47 points/m² was set to for consistency with existing lidar in the region (Cochran, 2016).

We conducted unmanned aerial vehicle (UAV) aerial photography surveys in fall of 2016 using a DJI Phantom 3 Advanced Quadcopter, using both manual and autonomous methods for acquiring photographs. The UAV is equipped with a 12.4-megapixel camera attached to a three-axis gimbal (angular control accuracy of ±0.02°). The camera lens has a focal length of 20 mm (35 mm format equivalent) and aperture of *f*/2.8. Although the altitude above ground level varied due to topography, an average altitude of 50 m was necessary for the desired decimeter-scale resolution. Within Lone Valley, five surveys were collected along the southwestern side of the valley and combined during processing, totaling ~3400 photos and ~0.80 km² (Table 1). Along the northeastern side of the valley, two surveys were combined, totaling 748 photos and ~0.27 km² (see the Supplemental Material[1]). Along the Lake Peak fault, the survey totaled ~780 photos for an area of ~0.26 km² (Table 1). Each individual survey totaled 20 min of flight time, with photographs taken at varying degrees of tilt to ensure high-resolution texture mapping in the later stages of processing. Ground control points were evenly spaced throughout the survey area and were recorded using a Garmin handheld GPS unit and verified where necessary using Google Earth satellite imagery.

We conducted surficial field mapping of survey areas at 1:2000 scale using traditional methods. Mapping of alluvial surfaces was based on sediment lithology, elevation, and channel incision. We also described alluvium and soil weathering profiles in local soil pits. Scarp and stream profiles were constructed later using digital elevation models (DEMs) derived from the aerial photography. We also excavated the cutbank of an ephemeral channel on the southwestern side of Lone Valley where

TABLE 1. UNMANNED AERIAL VEHICLE SURVEY DATA MODELING PARAMETERS AND RESULTS

Site	Model area (m²)	Number of images	Number of ground control points	Point density (points/m²)	Ground resolution (m/pixel)	Digital surface model resolution (m/pixel)	Root-mean-squared error (m)
Lone Valley site	804,000	3372	43	519	0.022	0.044	0.83
Lake Peak site	260,000	780	9	292	0.029	0.058	2.12
Gully cutbank	39.4	223	–	1.17×10^9	0.000463	0.000926	–

Note: Dash delineates that there is no value for that specific cell.

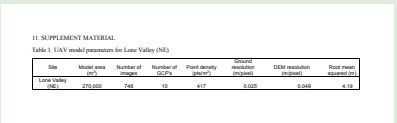
11. SUPPLEMENT MATERIAL

Table 1. UAV model parameters for Lone Valley (NE)

Site	Model area (m²)	Number of images	Number of GCPs	Point density (pts/m²)	Ground resolution (m/pixel)	DEM resolution (m/pixel)	Root mean squared (m)
Lone Valley (NE)	270,000	748	10	417	0.025	0.049	4.19

[1]Supplemental Material. Table of unmanned aerial vehicle (UAV) parameters for NE side of Lone Valley, and four uninterpreted UAV and lidar topographic hillshade models. Please visit https://doi.org/10.1130/GEOS.S.12210251 to access the supplemental material, and contact editing@geosociety.org with any questions.

potentially faulted alluvium was observed. A photomosaic was digitized using a 12-megapixel Pentax WG-3 GPS field camera (focal length 4.5 mm) and used as a base map for mapping the exposed alluvial stratigraphy.

Data Processing

Raw lidar data were processed by NCALM and are available on the OpenTopography website (www.opentopography.org). Both DEMs and digital surface models were generated by NCALM from point-classified lidar data, based on the time of return for each laser pulse (i.e., first return = vegetation canopy; last return = ground). We further processed the 1-m-resolution DEMs in ESRI ArcMap 10.5 software to generate 1-m-resolution shaded-relief maps. A strip map was generated from the final product along the Lake Peak fault for surficial mapping in ArcMap. For further information on processing lidar data, see the NCALM website (ncalm.cive.uh.edu).

We processed aerial photographs using structure-from-motion technology (Ullman, 1979). This method applies robust computer algorithms to traditional stereo photogrammetric techniques, whereby overlapping photographs are processed to create millions of three-dimensional (3-D) surface points (Lowe, 2004; Snavely et al., 2007). The "structure" (i.e., topography and color) of the ground-surface scene, as well as the camera position and orientation, are reconstructed using overlapping photographs from multiple angles (e.g., Johnson et al., 2014). Structure from motion is currently used for various applications, including 3-D surface reconstruction of simple objects, paleoseismology (Bemis et al., 2014; Reitman et al., 2015), and neotectonics (Johnson et al., 2014; Westoby et al., 2012). We constructed digital surface models of survey areas using Agisoft PhotoScan Pro software. Dense point clouds were generated by creating triangulated irregular networks (TINs), following the methods of Johnson et al. (2014). Using the default settings, we maximized the face count to produce surface models with ~5 cm/pixel resolution (Table 1). In each model, we classified the point cloud to remove the vegetation by iteratively changing the height-above-ground (0.1–1.0 m) and angle (0°–45°) parameters (defined relative to the model-determined ground points) until an optimal surface model resulted. The best resulting parameters in all surveys were 0.1 m height above ground and 15° surface angle. Based on ground truthing, these values remove the most vegetation while preserving underlying surface topography. Following this approach, digital surface models were thereby transformed into true DEMs for interpretation of fault location and neotectonic activity. We followed a similar approach for creation of surface models at sub-millimeter-per-pixel resolution from digital, ground-based photographs of the potential fault exposure in Lone Valley.

RESULTS

Lone Valley

Across Lone Valley, there are three likely locations for active strike-slip faulting: (1) the linear escarpment of the eastern edge of the Big Bear block that forms the western boundary of the valley, (2) the sharp eastern edge of the valley along Granite Peak, and/or (3) across the middle of the valley where Miller and Cossette (2004) mapped a northwest-trending fault cutting bedrock and Holocene deposits (Fig. 3). Despite the sharpness of the eastern valley margin near Granite Peak, a high-resolution DEM based on structure-from-motion analysis shows no geomorphic evidence for faulting (see the Supplemental Material [footnote 1]). The slope break consists of coarse-grained, loose granitic colluvium that is banked up against the linear edge of triangular facets. The form of these deposits is typically smooth and unbroken by scarps. Ephemeral drainages across these deposits appear undeflected. We therefore conclude that if the eastern margin of Lone Valley is faulted, the fault has not been active recently enough to disturb depositional and erosional surfaces that are present.

More evidence of recent faulting is present in the center of Lone Valley. The high-resolution DEM shows that mapped fault traces locally appear as discontinuous, en echelon lineaments (Fig. 4B), which Miller and Cossette (2004) interpreted to cut across both Pennsylvanian bedrock (unit Pbu) and Holocene alluvium (Fig. 4A). These lineaments are also visible in aerial photographs on the basis of color changes and lineations, but only in a few locations correspond to scarps demarcating elevation steps of 6–8 m in the DEM (Fig. 4B). These topographic steps occur in either Pennsylvanian bedrock only or where bedrock meets Quaternary alluvium (Fig. 4A). The alluvial surfaces (units Qf, Qa, Qyf, Qyf1, Qyf3) along the fault include higher, more-incised surfaces of matrix-supported, fine-grained sediments of carbonate, feldspar, and granitic lithology and a prominent K horizon with platy structure. Between these are lower surfaces that consist of fine-grained, loose, structureless alluvium. Dense vegetation including juniper and Joshua trees also causes root disturbance and valley-floor clutter, making fault investigation difficult due to low visibility. Because of the high sand and low clay content of this carbonate-rich alluvium, as well as the lack of a well-developed K horizon, this surface is soft and does not preserve channel edges or other features. This may in part explain the lack of a well-developed scarp in Quaternary alluvium along the proposed fault. Although Miller and Cossette (2004) mapped discrete faulted bedrock domains and a sequence of alluvial surfaces, in most cases it was not possible to systematically relate these surface classifications to geomorphic features observable in the high-resolution DEM or in the field. Additional evidence for faulting along this weakly defined lineament is the deflection of numerous northeast-running streams (Fig. 4B). These deflections are typically on the order of 20–25 m and would correspond to right-lateral motion on the fault (if true offsets). Given the ambiguity in these deflections, the fact that other streams are not deflected, and the lack of ages on the relevant alluvial surfaces, we hesitate to interpret true lateral offset or speculate on slip rate based on these observations.

We observed additional evidence for faulting along this weakly defined lineament in a single exposure. Within a cutbank of a stream channel, we excavated and documented sharp discontinuities

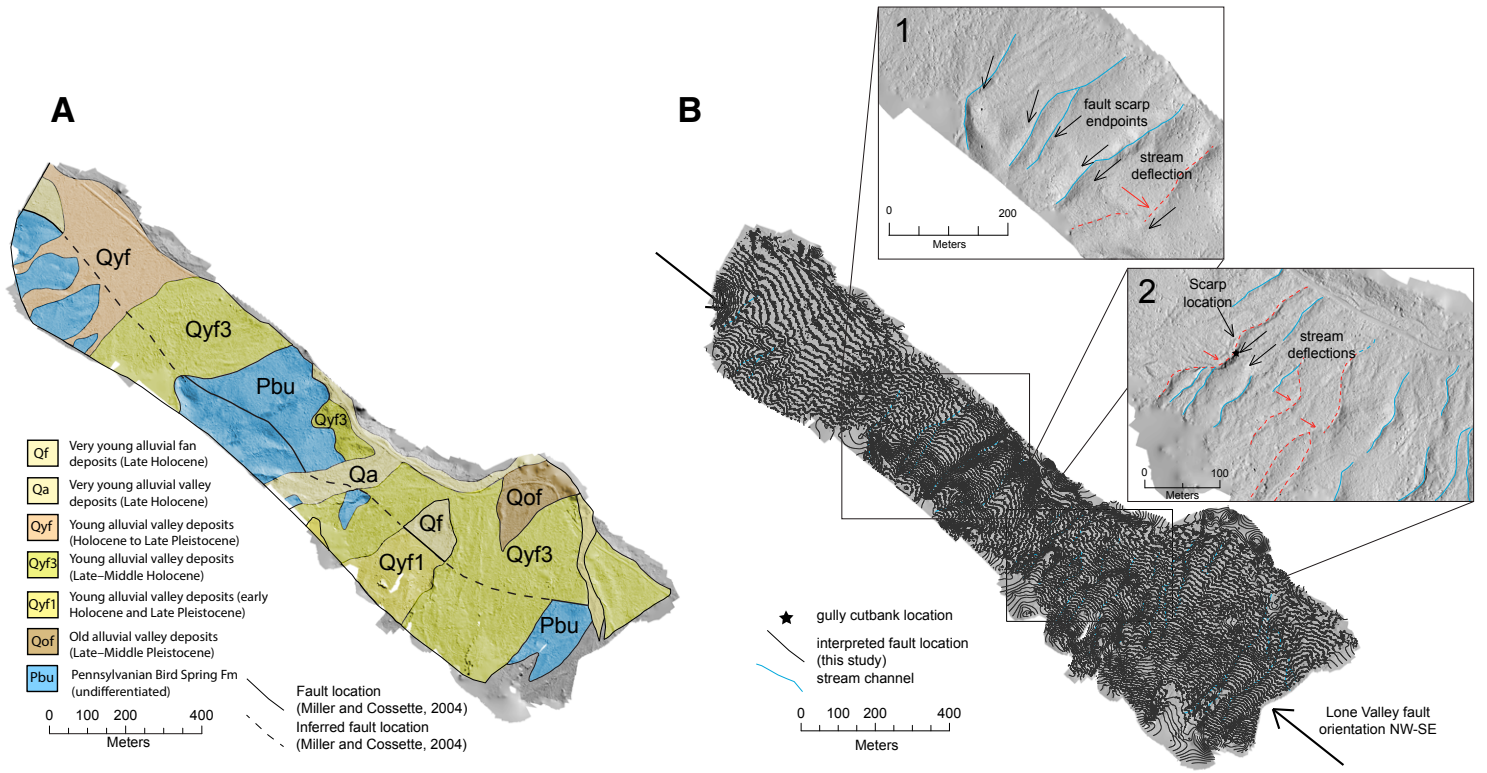

Figure 4. Lone Valley fault southwest site (see Fig. 3). (A) Bedrock and surficial geology previously mapped by Miller and Cossette (2004) indicating Quaternary-age faulting that cut across several young alluvial surfaces. (B) High-resolution shaded relief derived from our unmanned aerial vehicle (UAV) survey data, overlain by a 1 m contour map derived from the UAV digital elevation model. Black lines represent interpreted faults based on lineaments found in the shaded relief from this study. The star is the location of Figure 5. Ephemeral stream channels were traced based on contours and show a series of deflected channels (insets 1 and 2). Insets 1 and 2 show end points for topographic step locations (black arrows) and deflected stream channels (red dashed lines). For an uninterpreted UAV shaded relief, please see Figure S2 in the Supplemental Material (text footnote 1).

and potential offsets of alluvial beds (Fig. 5). The steep, southwest-dipping contact juxtaposes coarse-grained, poorly sorted gravels (i.e., coarse sand to boulder sized) and white, well-sorted fine sand and clay. Rotated clasts within the coarse-grained gravel and laminated wedge-shaped deposits of coarse sand occur along the contact. Below the coarse-grained gravel, white laminae of clay and fine sand appear to be relatively continuous across the downward projection of the discontinuity. These layers were found to be lenses in three dimensions, and we were unable to map distinct, stratigraphic horizons across the discontinuity. Although we did not trace the discontinuity to a master fault below these lenses, we hypothesize that deeper excavation at this site might reveal a clearly defined fault. While the termination and juxtaposition of layers along this contact could be interpreted as depositional (i.e., a buttress unconformity), the current drainage direction is orthogonal to the contact, and the colocation with the lineament and deflected streams suggests a plausible tectonic origin.

The tectonic geomorphology of Lone Valley is thus somewhat ambiguous. Features across the center of the valley are roughly consistent with recent right-lateral faulting, suggesting a southeastward continuation of the Helendale fault. The minimal evidence for faulting may, however, imply a low rate of neotectonic activity. Alternatively, the poor topographic expression of this fault may be due to the poor preservation capacity of the loose deposits and vegetated surfaces of the valley.

Lake Peak

The discontinuous, en echelon trace of the Lake Peak fault is clearly visible in the lidar shaded relief

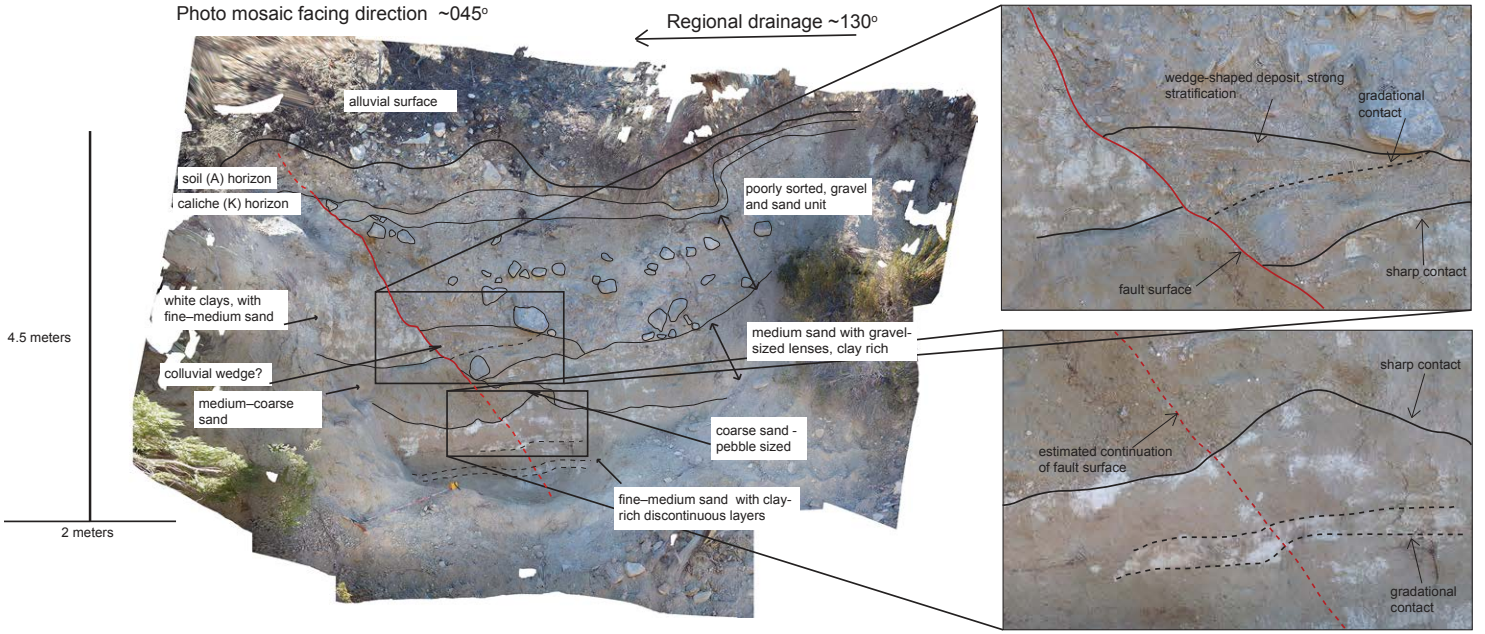

Figure 5. Photomosaic, created using Agisoft PhotoScan software, of a cutbank within an ephemeral stream along the southwestern side of Lone Valley (see Fig. 4B for location). A clear discontinuity exists between coarse, poorly sorted gravel and fine to medium sand and white clay (red line). Upper right inset shows potential colluvial wedge deposits forming right at the contact between these two units. No true master fault could be found at depth, and could potentially be lost in the finer-grained, massive unit at the base of our excavation (lower right panel). Black lines represent contacts between the sediment packages mapped during field work; dashed lines are gradational contacts, and solid lines are sharp contacts.

of the North Fork Whitewater River drainage near San Gorgonio Mountain (Fig. 6). The fault trace begins north of the convergence of the Mill Creek, Mission Creek, and Pinto Mountain faults in Hell For Sure Canyon, 2.5 km north of the Mill Creek fault, and is mappable for ~10 km northwestward to Dollar Lake. In the North Fork Whitewater River valley, the fault appears as a dark lineament on the northern flank of the valley above the trunk stream. Although this fault clearly cuts across numerous tributary gullies, there are no clear lateral offsets (Figs. 7, 8). To the northwest, the fault continues as en echelon scarps into higher elevation and cuts glacial deposits. These deposits have been mapped and dated as sharp-crested, nested end moraines and recessional loops created by cirque glaciers during the Wisconsin glaciation (Sharp et al., 1959). The fault scarp is tall (as much as ~20 m) and well defined in these coarse deposits (Figs. 9C–9D). The fault is also visible as lineaments in older alluvium that occurs between deposits, although is not visible in active washes (Figs. 8A–8D). To the northwest of the Mine Shaft Saddle, the fault continues through complex, lobate glacial deposits of the Dry Lake and Dollar Lake glaciers, but is locally lost in the complex ribbed, hummocky topography of the lower glacial deposits (Fig. 8A).

Geomorphic mapping of the fault through these deposits based on high-resolution topography and field observations indicates that the fault has likely ruptured in the Late Pleistocene (Figs. 7, 8, 9). The fault scarp occurs within mapped glacial deposits that are dated as ca. 12–16 ka based on cosmogenic dating (Owen et al., 2003). Due to the hummocky topography of these deposits and their coarse nature (typical boulder size ~1 m), there are no clear preserved offsets of geomorphic features, such as moraine edges or crests. These deposits are also locally mantled by coarse colluvium and talus derived from San Gorgonio Mountain, further obscuring interpretation of offsets (Figs. 8A–8B).

The higher-resolution DEM from structure-from-motion analysis of the North Fork Whitewater River glacier deposits shows the surface complexity of the deposits in more detail (Fig. 9A). The apparent height of the scarp through this moraine is ~22 m, but this is exaggerated due to the original steep slope of the faulted material, distance between the preserved offset surfaces on either side of the scarp, as well as addition of boulders to the upper slope (Fig. 9C). The actual vertical separation across the fault is 9 ± 3 m, as measured based on the offset of the tilted depositional surface using the high-resolution topographic profile (Fig. 9C). It

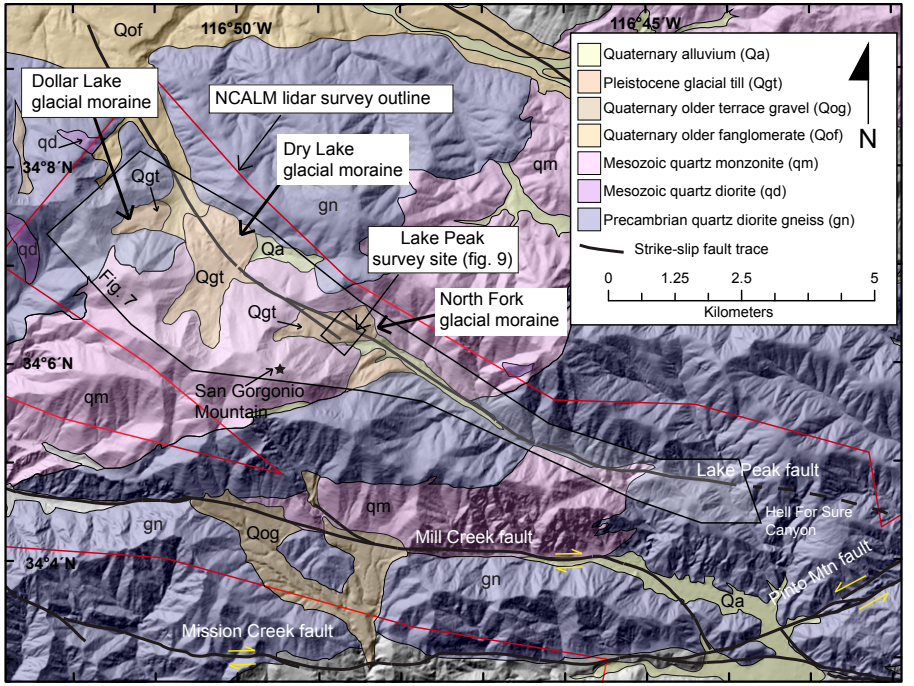

Figure 6. Bedrock geology map modified from Dibblee (1964b) overlaid on a 1/3-arc-second digital elevation model–derived shaded relief. Locations of the Lake Peak, Mill Creek, Mission Creek, and Pinto Mountain faults (black lines) form a nexus of converging strike-slip faults in the Whitewater River watershed. Red outline shows the extent of our National Center for Airborne Laser Mapping (NCALM) lidar survey in the San Bernardino Mountains, which is publicly available at www.opentopography.org. Black-outlined transparent strip is the location of the strip map in Figure 7. The Lake Peak fault can be seen cutting across the three glacial deposits, namely the North Fork, Dry Lake, and Dollar Lake glacial moraines.

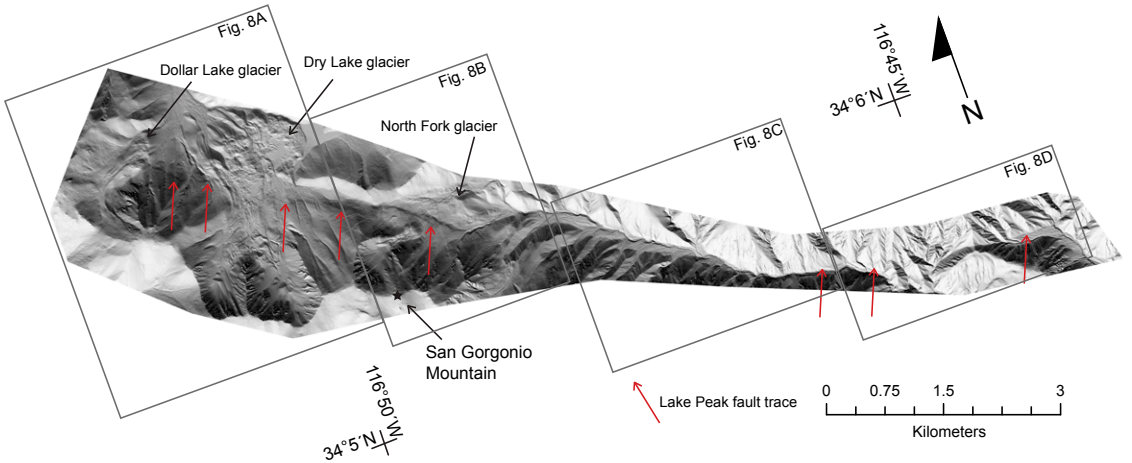

Figure 7. One-meter digital elevation model–derived shaded relief (lighting direction 090°) map of North Fork Whitewater River drainage showing the locations of several fault scarps of the Lake Peak fault (red arrows). Four panels were cut, from northwest (Fig. 8A) to southeast (Fig. 8D), from this shaded relief and used as the basis for geomorphic mapping. The Dollar Lake, Dry Lake, and North Fork glacial moraines were originally described by Sharp et al. (1959). Radiometric ages (see Figs. 8A–8B for location) for each of these glaciers were produced using cosmogenic nuclides and are originally from Owen et al. (2003).

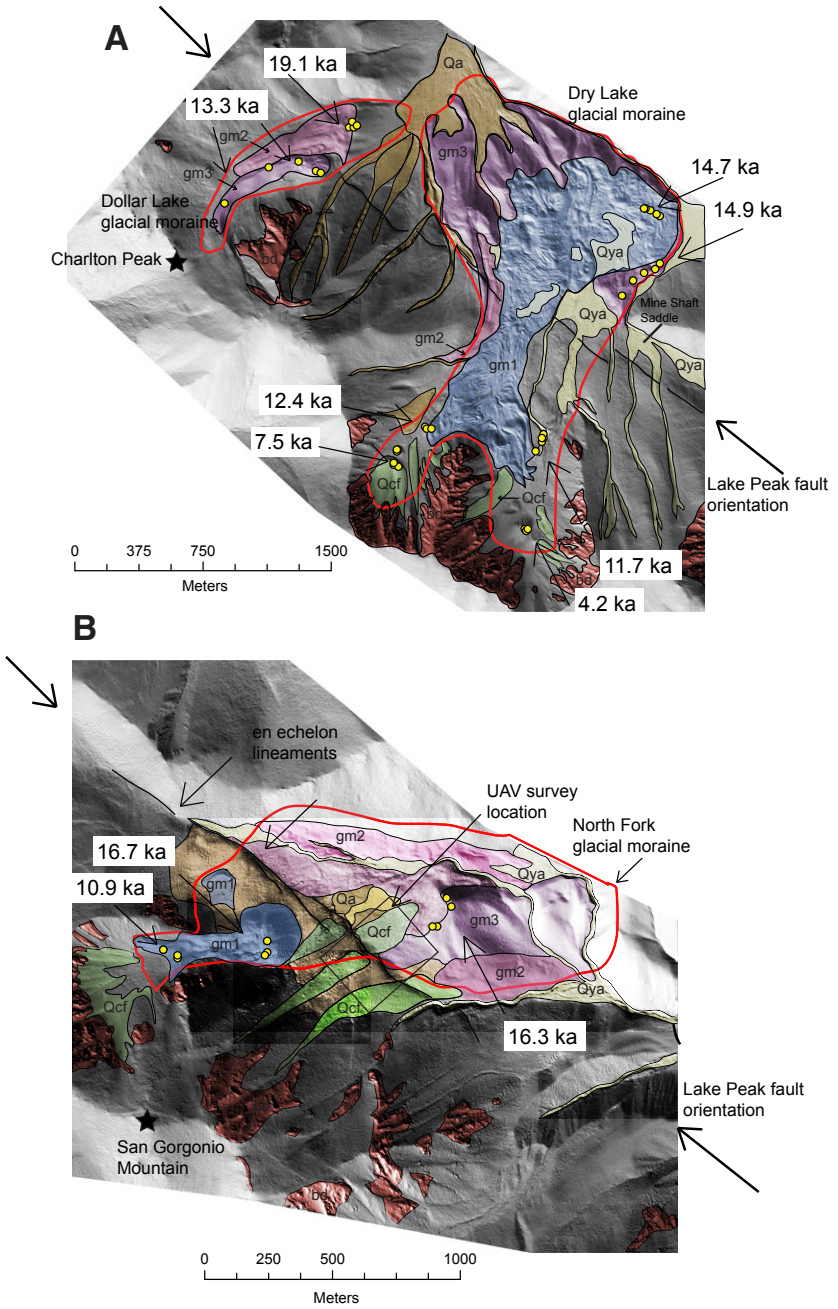

Figure 8. Four panels (A–D) were clipped from the lidar shaded relief and used as a basis for geomorphic mapping (see Fig. 7). Mapping was based on field evidence, surface elevation, and geomorphology of the surface (e.g., hummocky, ribbed, etc.). The Lake Peak fault trace is en echelon and discontinuous. Yellow dots represent average cosmogenic ages grouped together by location. Original ages were produced by Owen et al. (2003). Black lines represent interpreted fault lineaments from this study. Red outlines in A and B are the extent of the glacial moraines mapped by Sharp et al. (1959). (A) Geomorphic mapping of the Dry Lake and Dollar Lake glacial moraines showing the fault lineaments crossing both the glacial deposits and the young alluvium. (B) Surficial geology mapping of the North Fork glacial moraine suggests multiple periods of deposition of young colluvium since glacial retreat in the Pleistocene. UAV—unmanned aerial vehicle. (C and D) Mapping based solely on the lidar, indicating discontinuous lineaments throughout the North Fork Whitewater River drainage. Uninterpreted panels A–D can be found in the Supplemental Material (text footnote 1).

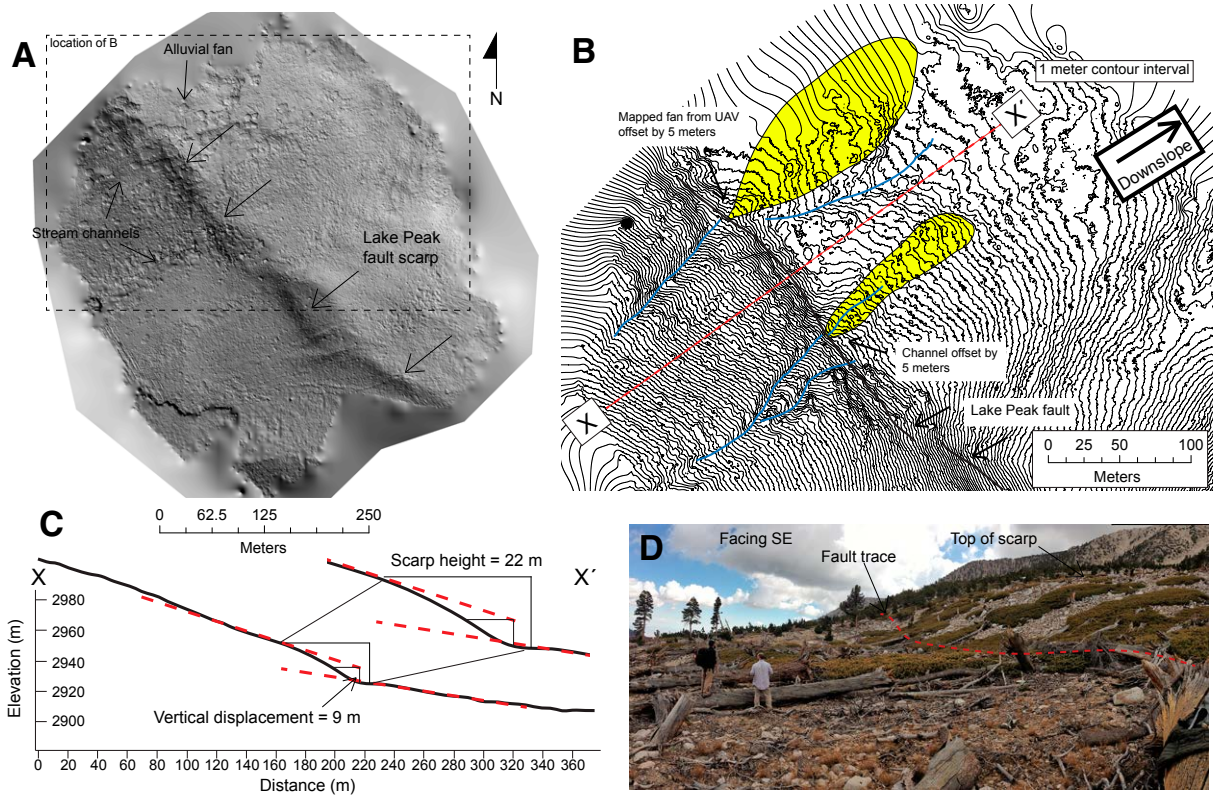

Figure 9. Lake Peak unmanned aerial vehicle (UAV) survey site (Figs. 6 and 8B). Two surveys using manual flight mode were combined for generation of a surface model along the fault scarp. (A) UAV digital elevation model (5 cm resolution)–derived shaded relief (lighting direction from southwest). Points were classified using Agisoft PhotoScan software parameters 0.10 m and 15°. As a result, the model was interpolated across the areas where vegetation was removed, which can leave a "lunar surface". At the resolution we have obtained, little information is lost during point classification. Scarp is indicated by black arrows. (B) One-meter contour map showing interpretation from our high-resolution topography. Two 5 m offsets are interpreted at the front of the fault scarp: (1) a feature interpreted as the apex of an alluvial fan is matched to the mouth of the channel to the northwest, and (2) a channel is dextrally offset across the scarp based on topographic contours and field evidence. (C) Profile of the Lake Peak scarp (see B for location) showing the magnitude of both the total scarp height and the vertical separation. The vertical separation assumes that the near-vertical fault is located at the toe of the scarp. Red dashed lines indicate the upslope and downslope surface extensions used for estimating the vertical separation of the scarp. (D). Field photo (34°6′21″N, 116°48′54″W) facing southeast showing the magnitude of the fault scarp and the loose, poorly defined nature of the deposits that are cut by the fault.

is unclear whether local normal or reverse motion formed the scarp. The height of the scarp may also be accentuated by surface collapse and slumping of the glacial deposits, although the linear nature of the scarp suggests origin primarily by faulting. Because of the coarseness of the boulder moraine deposits, there are no clearly defined channels or levee deposits to check for lateral displacement. However, we documented two possible horizontal offsets of ~5 m (right lateral) of stream channels that cut through the moraine and their respective fan deposits downstream (Fig. 9B). These channels are well defined uphill of the scarp but do not continue to the east of the fault (Figs. 9A–9B). The proposed offsets are therefore based on the separation of these channels from the apex of lobate fan deposits of coarse alluvium derived from the eroding moraines (Fig. 9B). We delineated these fans in the field based on surface relief, the color of fine-grained matrix, and lateral variations in grain size. These slip estimates are speculative, however, and because of the ambiguity in the interpretation, it is not possible to quantify uncertainties for the offset itself. While the measurements of horizontal

distance were made to within ~1 m using tape measure, the true uncertainties in the offset are likely greater than the offset itself. It is unclear whether more conclusive determinations could be made given the loose nature and rapid erosion of these coarse deposits.

Figure 9D illustrates how unstable this intermontane valley is due to the steep, eroding landscape, particularly so close (<1 km) to San Gorgonio Mountain (Fig. 8B). Our mapping indicates that loose colluvium is consistently being deposited atop the glacial moraines, obscuring the true nature of fault expression, and estimation of fault offsets may be better suited to the northwest near Dry Lake or Dollar Lake glaciers. If these horizontal offsets are valid, however, they would suggest a minimum right-lateral slip rate of 0.3 mm/yr (0.6 ± 0.2 mm/yr vertical slip rate) based on the age of the glacial deposits. The uncertainties in the horizontal slip rate estimate exceeds the actual value, however.

DISCUSSION

Evidence for Strike-Slip Faulting in the San Bernardino Mountains

Our results provide support for the hypothesis that dextral shear is transferred from the SAF to the ECSZ through the convergent zone of the SBM. Southward continuation of the Helendale fault as the Lone Valley fault into the Big Bear block appears at least plausible based on the newly acquired high-resolution topography. Although no conclusive evidence of Holocene strike-slip faulting was observed in Lone Valley, we do observe features that are consistent with strike-slip deformation of Pleistocene alluvial surfaces (Figs. 4–5). The evidence includes a potential exposure of faulted Pleistocene (?) gravels and discontinuous en echelon scarps that run through the valley (Fig. 5). These features, along with the sharp escarpments on both sides of the valley and the proximity and parallelism to the southern Helendale fault, suggest that the Lone Valley fault is likely a connection between the Helendale fault and the Pipes Canyon fault to the southeast (Fig. 2). The evidence for active dextral slip along the Lake Peak fault is less ambiguous. High-resolution topography clearly delineates numerous scarps cutting Late Pleistocene glacial deposits. Apparent vertical offset along one of these scarps implies significant fault motion at a rate of 0.5–1 mm/yr. Although inconclusive, right-lateral deflections along this scarp are also consistent with dextral slip rates on the order of 0.3 mm/yr. The offsets and potential rates that we present are uncertain, however, and should not be quoted as robust measurements of fault activity. We estimate conservatively that uncertainties in these estimates should exceed the actual slip rate value (i.e., >100%), but they are not directly quantifiable.

Given that both faults occur within erosional terrain and are manifest in unstable, coarse, vegetated deposits without well-defined depositional surfaces or well-preserved channels or other features, the moderate evidence for recent motion along them may underrepresent their true activity. Whereas active faults with ~1 mm/yr dextral motion in the southern ECSZ are well preserved and easily mapped in the Mojave Desert (Oskin et al., 2008), we speculate that faults of similar activity could be masked by the unstable, eroding terrain across the high SBM. The lack of well-preserved depositional surfaces in the SBM across these faults also means that we cannot rule out or disprove the possibility that they have experienced Holocene displacement. Because of the evidence we observe for dextral motion on these faults, and considering the preservational bias of the terrain, we interpret that these faults represent active strands of the ECSZ.

Other locations within the SBM provide additional evidence of active dextral faulting. The Pipes Canyon fault exhibits apparent dextral offsets of 1.8 km of both the bedrock-incised Pipes Canyon and an alluvial fan to the northwest (Figs. 10C–10D). Neither offset has been dated or accurately measured and defined with field data, however. The Deer Creek fault occurs along strike of the Lake Peak fault to the north and also displays evidence for Quaternary displacement (Spotila and Sieh, 2000) (Fig. 10A). This evidence includes a 200 m dextral offset of the Pliocene Santa Ana thrust and linear valley which coincide with the Deer Creek fault, although there is no apparent continuation to the northwest (Dibblee, 1964b; Jacobs, 1982). Other shorter and more ambiguous high-angle faults occur within the SBM, not all of which have been mapped. For example, a linear northeast-trending valley that cuts across the grain of lithology and the southern escarpment of the Big Bear plateau occurs in the vicinity of the 1992 M_w 6.5 Big Bear aftershock sequence (Jones and Hough, 1995) (Figs. 2, 10B). Although no offsets have been mapped along this feature, it appears tectonic in nature and may be related to the left-lateral source of faulting that produced this earthquake. Such conjugate left-lateral faults, which would likely be nascent given their poor topographic expression, may combine with the discontinuous right-lateral faults to accommodate significant penetrative strain in the Big Bear block (i.e., quasi-pure shear, after Yeats et al. [1997]).

Kinematic Interpretation

The presence of strike-slip faulting in the SBM, a primarily thrust-dominated convergent zone, requires a kinematic explanation. Spotila and Anderson (2004) previously interpreted this deformation system in the context of advection of a convergent zone around a fault bend and into a realm of dextral shear. They hypothesized that as the convergent blocks of the SBM advect eastward around San Gorgonio Pass, they enter into the dextral faulting domain of the ECSZ (Figs. 1, 11). In this regard, the ECSZ appears to propagate westward into what was formerly a compressional domain. This model was inspired by observations implying that the eastern North Frontal thrust system exhibits much less evidence for recent activity than the Holocene active thrust system to the west of the Helendale fault, suggesting that the thrust system is becoming progressively shut off as the ECSZ slices westward into it (Fig. 11). The domain of strike-slip faulting was hypothesized to occur east of a line projecting between the Helendale fault and the inflection point in the Coachella Valley segment of the SAF, between more westerly trending (to the northwest) and more northerly trending (to the southeast) faults (Fig. 11). Such a model of

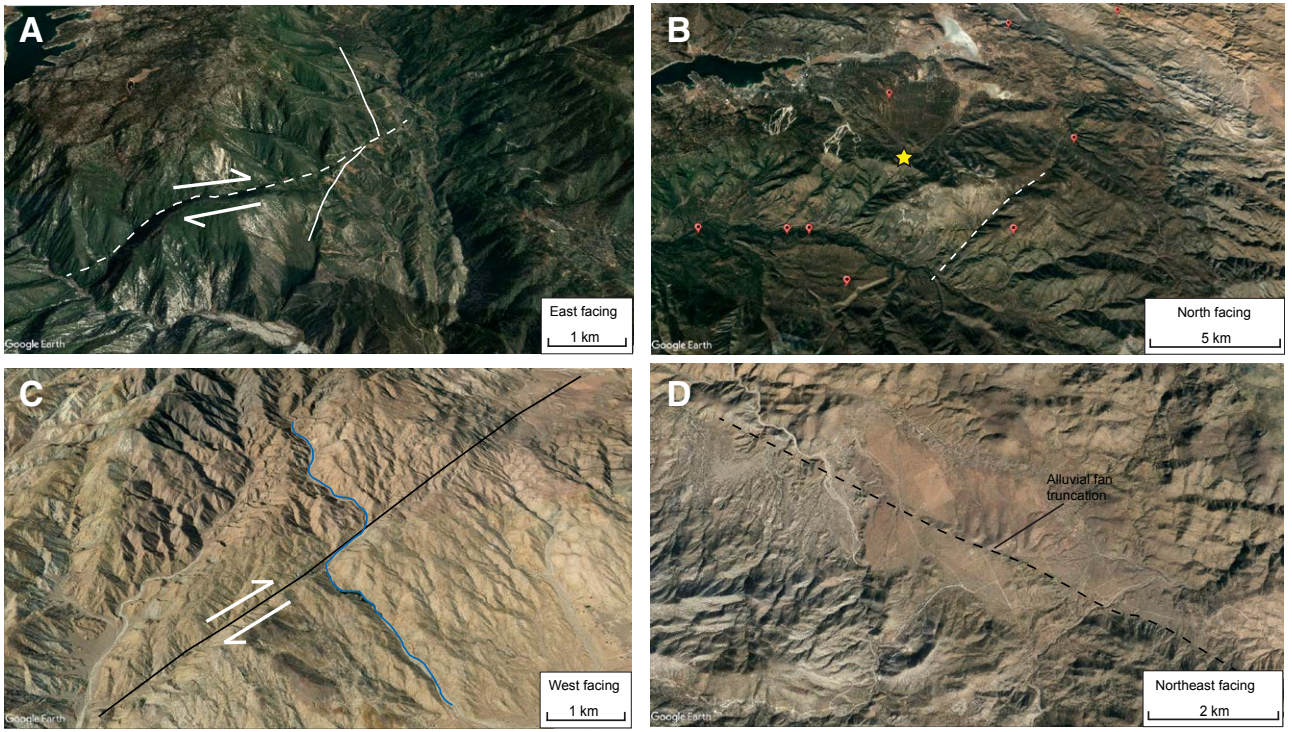

Figure 10. Google Earth images of various locations within the San Bernardino Mountains (SBM) showing evidence for strike-slip faulting. (A) Mapped 200 m offset of the Santa Ana thrust (white solid line) across the Deer Creek fault (Dibblee, 1964b; Jacobs, 1982). (B) Linear valley along strike of the overall trend of the 1992 Big Bear aftershock epicentral locations (yellow star—main shock; red markers—aftershocks taken from Jones and Hough [1995]), which may represent the surface expression of the fault responsible for the Big Bear aftershock sequence. (C and D) Pipes Canyon fault indicates a channel deflected by 1.8 km (blue line in C), and a lineament (dashed black line in D) that truncates the apex of an alluvial fan with an apparent offset of ~1 km from the large drainage to the northwest. The fault kinematics of these locations is unknown and should be the focus of future neotectonic studies within the SBM.

advecting deformation zones alongside a restraining bend has been recognized along other sections of the SAF as well as other fault systems (Anderson, 1990; Bemis et al., 2015; Benowitz et al., 2011; Burkett et al., 2016; Buscher and Spotila, 2007; Meisling and Weldon, 1989; Schwartz et al., 1990; Wakabayashi, 2007). Given that strike-slip faults, namely the Lake Peak and Deer Creek faults, occur to the west of this line, however, this model may not fully explain the deformation pattern in the SBM.

We propose a revised model in which strike-slip faulting of the ECSZ penetrates farther west of the Helendale–Pipes Canyon fault into the still-active SBM convergent domain. While convergence may be the result of the double restraining bend at San Gorgonio Pass (Spotila and Sieh, 2000), dextral slip may be overprinting convergence due to excessive dextral strain between the San Bernardino strand of the SAF and fully active ECSZ farther to the east. The dextral faulting may still be influenced by the restraining bend, however, given that the strike-slip faults seem to fan around the bend from a point near Desert Hot Springs (Figs. 2, 11). The discontinuous strike-slip faults in the SBM rotate from more northerly trending to more westerly trending from east to west, from the Johnson Valley fault, to the Pipes Canyon fault, to the Lone Valley fault, and to the Lake Peak–Deer Creek fault (Fig. 2). This may indicate that the stress field rotates around the restraining bend. This may be analogous to the rotation of strike-slip faults around indenter corners, as has been observed in southeast Asia around the Indian indenter (Morley et al., 2007). Such a fanning of faults has been explained mechanically as the slip lines of maximum shear stress in a deforming plastic material (Molnar and Tapponnier, 1977; Tapponnier and Molnar, 1976). Although the mechanics of this model are not analogous, slip-line theory at least provides a conceptual explanation for why the

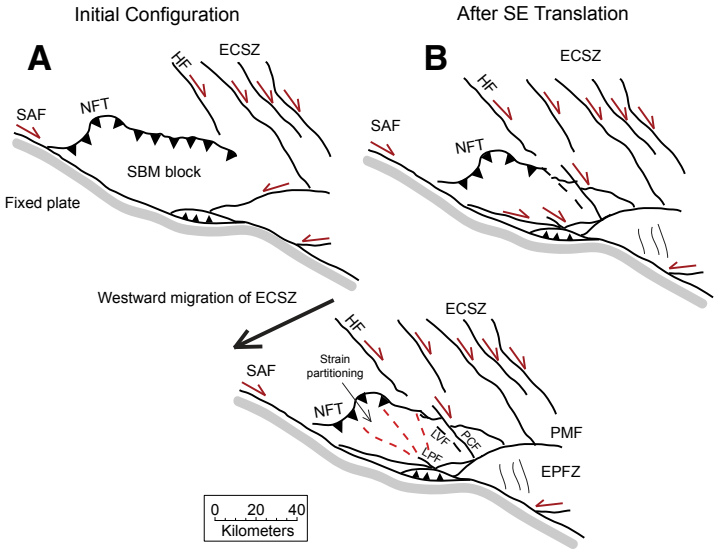

Figure 11. Dextral-overprinting model showing the westward migration of the Eastern California shear zone (ECSZ). (A) An interpretation for the initial configuration of the San Bernardino Mountains (SBM) prior to southeastward translation into the ECSZ. The entire North Frontal thrust (NFT) was active as a purely convergent zone of deformation. (B) After the SBM has translated to the southeast via the San Andreas fault (SAF), dextral overprinting of the ECSZ begins to "slice" the NFT and SBM due to excessive strain along the convergent margins. The bottom figure shows the current fault configuration, with strain partitioning occurring throughout the SBM west of the Helendale fault (HF). Similarly to ECSZ faults, the faults within the SBM also become more northerly trending toward the east, and more westerly trending toward the west. EPFZ—Eureka Peak fault zone; LPF—Lake Peak fault; LVF—Lone Valley fault; PCF—Pipes Canyon fault; PMF – Pinto Mountain fault.

strike-slip faults in the SBM may progressively fan around San Gorgonio Pass.

If this model is correct, it implies that the strike-slip faults within the SBM need not postdate convergence, but rather that dextral slip may overprint reverse faulting of the convergent zone in a complex pattern of strain partitioning. Whether these discontinuous strike-slip faults are nascent, as originally suggested by Spotila and Anderson (2004), is unclear. While it is logical that these faults are discontinuous because they have just formed due to westward migration of the ECSZ into the convergent domain, this is not required. The model also implies that the diffuse strike-slip faults of the SBM may thus be important for accommodating regional dextral strain, similar to the other faults of the ECSZ, and in fact may effectively be a southwestward continuation of the ECSZ. This implies that there is direct transfer of dextral strain between the SAF and the ECSZ along the zone between San Gorgonio Pass and Cajon Pass. This would make the westernmost ECSZ unique because the connection between these fault systems is more complex farther east along the eastern Transverse Ranges, including conjugate left-lateral faults (i.e., Pinto Mountain fault) and vertical-axis block rotation (Fig. 1).

Implications

While Holocene motion is inconclusive along the Lone Valley fault, the potential for this fault acting as a connecting fault between the Helendale fault to the north and the Pipes Canyon fault to the south is important for earthquake hazards. Using the style of the 1992 Landers (California) earthquake rupture as a model (Sieh et al., 1993; Wald and Heaton, 1994), the total fault length from the Pipes Canyon, through the Lone Valley, and onto the Helendale fault is >50 km. Based on the scaling relationships between surface rupture length and moment magnitude, this equates to a M_w 7.0 earthquake (Wells and Coppersmith, 1994). Holocene rupture on the Lake Peak fault seems plausible given the presence of scarps and displacements along its trace. As mapped, the Lake Peak fault is ~10 km in length, which equates to ~1 m of maximum displacement per rupture (Wells and Coppersmith, 1994). This suggests that multiple events have occurred on the Lake Peak fault since the Pleistocene, with the potential for a minimum M_w 6.5 earthquake occurring if only this fault length ruptures (Wells and Coppersmith, 1994). Given its proximity to the SAF and the possibility that it continues to the northwest as the Deer Creek fault, we suggest that the Lake Peak fault should be considered as an active fault and considered in models of strain accumulation and stress evolution associated with San Gorgonio Pass. The possibility of activity on the Lone Valley and Lake Peak faults may also be higher than would otherwise be estimated for their topographic expressions, given that the local high topographic relief is less likely to preserve a record of active faulting than nearby depositional environments, such as the Mojave Desert or Los Angeles Basin.

Another implication involves the slip-rate discrepancy between geologically and geodetically determined fault kinematics between the ECSZ and the SAF, and how this may be resolved if dextral faults within the SBM were added into the overall slip budget. Geodetically determined slip rates for the southern ECSZ are suggested to sum to ~15 mm/yr for all of the main faults (i.e., Helendale, Camp Rock, Calico, Lenwood, Ludlow, Johnson Valley, Emerson, and Pisgah-Bullion faults) (McGill et al., 2015; Meade and Hager, 2005; Spinler et al., 2010), two to three times larger than the sum of the Late Pleistocene slip rate of ~6 mm/yr across

the same faults (Oskin et al., 2008). McGill et al. (2015) modeled transects across all major faults east and west of the San Jacinto fault, with a total slip budget of ~47 mm/yr, which is ~7 mm/yr less than the ~54 mm/yr of slip between the North American and Pacific plates (DeMets and Dixon, 1999). While permanent, off-fault deformation may be a contributing factor in the total slip deficit, our results suggest that smaller, nascent faults must also be accounted for.

The occurrence of strike-slip faults in the SBM is an illustration of the complexity of the connection of the ECSZ to the SAF north of San Gorgonio Pass. The discontinuous faults of the SBM may accommodate a fraction of the right-lateral slip that has been observed as missing along the SAF in San Gorgonio Pass. Kendrick et al. (2015) suggested that faults within San Gorgonio Pass must accommodate all dextral slip transferred from the Banning fault strand of the SAF in the south to the San Bernardino strand of the SAF in the north, because the Mill Creek and Mission Creek faults have been inactive since the Pleistocene. Yet thrust faults within San Gorgonio Pass appear to accommodate only a fraction of the motion (Heermance and Yule, 2017; Yule and Sieh, 2003). Distributed strain on shorter structures outside of San Gorgonio Pass, such as the Lake Peak fault, Morongo Valley fault, or Pipes Canyon–Lone Valley fault, may thus play an important role in accommodating the high strain that results from the double restraining bend in the SAF at San Gorgonio Pass.

A final implication of this research is recognition of the relative difficulty for estimating fault activity within a predominantly erosive geomorphic environment. Fault studies in the region generally involve mapping older depositional surfaces in which scarps and potentially offset features are well preserved, such as in the Mojave Desert (e.g., Oskin et al., 2007, 2008). Our results illustrate the challenges of working in mountainous terrain, including the occurrence of young, cohesionless, unstable sediment, with poor preservation potential due to the rapid (i.e., >0.1 mm/yr) erosion occurring within the study area (Spotila et al., 1998; Binnie et al., 2010). Additional challenges included poorly defined linear features used to define piercing points, and an absence of well-preserved depositional surfaces that can be used to quantify the duration of time since fault rupture. Prior work has not documented a reliable calibration of what tectonic geomorphology in mountain terrain translates to in terms of recent fault activity, making it difficult to compare to other settings and making it unclear what magnitude of fault activity in the SBM and other ranges may go undetected until rupture is observed.

CONCLUSIONS

Our results provide first-order evidence on incipient dextral strike-slip faulting within the SBM, focusing on two locations of previously mapped strike-slip faults that cut across Quaternary-age deposits. In Lone Valley, high-resolution UAV surveys reveal a series of deflected streams and 6–8-m-high topographic steps that cut through soft, loose alluvial sediments. The tectonic geomorphic expression, however, is somewhat ambiguous, and may reflect low rates of fault slip or a lack of preservation capacity of faulted landforms within the valley. The Lake Peak fault displays a prominent, ~9-m-high scarp that cuts across Pleistocene glacial deposits, though only speculative lateral offsets of ~5 m in alluvial fan deposits could be determined at the base of this scarp. The lack of a stronger geomorphic expression of offsets may be the result of the high rate of debris shed from the eroding San Gorgonio massif. While our focus on two faults within the SBM provides some evidence for dextral faulting, several other faults within the SBM also display strike-slip expressions (Sylvester, 1988). Linear valleys, deflected streams, and displaced ridges and alluvial fans suggest that diffuse strike-slip faulting is prevalent within the SBM. The existence of these faults suggests an evolution of stress regime in the SBM, from predominantly convergent to strike-slip, and may represent the southwestward migration of the ECSZ. Although our kinematic model explains how dextral overprinting may be occurring within the SBM, a more detailed documentation of fault kinematics in the SBM is necessary to understand how slip is transferred from the SAF to the ECSZ near San Gorgonio Pass.

ACKNOWLEDGMENTS

Michael Oskin and Zachery Lifton provided very insightful reviews that greatly improved the quality of this manuscript. We would like to thank the folks at Whitewater Nature Preserve for hospitality and help with discovering the best routes and trails to take to San Gorgonio Peak. We would like to thank NCALM seed proposal data collection and processing services provided by the OpenTopography Facility with support from the National Science Foundation (NSF) under NSF award numbers 1833703, 1833643, and 1833632. Support for this study was provided by NSF grant EAR-1145115 and NCALM seed proposal funding for flying the lidar survey.

REFERENCES CITED

Anderson, R.S., 1990, Evolution of the northern Santa Cruz Mountains by advection of crust past a San Andreas fault bend: Science, v. 249, p. 397–401, https://doi.org/10.1126/science.249.4967.397.

Andrew, J.E., and Walker, J.D., 2017, Path and amount of dextral fault slip in the Eastern California shear zone across the central Mojave Desert: Geological Society of America Bulletin, v. 129, p. 855–868, https://doi.org/10.1130/B31527.1.

Behr, W.M., Rood, D.H., Fletcher, K.E., Guzman, N., Finkel, R., Hanks, T.C., Hudnut, K.W., Kendrick, K.J., Platt, J.P., Sharp, W.D., Weldon, R.J., and Yule, J.D., 2010, Uncertainties in slip-rate estimates for the Mission Creek strand of the southern San Andreas fault at Biskra Palms Oasis, southern California: Geological Society of America Bulletin, v. 122, p. 1360–1377, https://doi.org/10.1130/B30020.1.

Bemis, S.P., Micklethwaite, S., Turner, D., James, M.R., Akciz, S., Thiele, S.T., and Bangash, H.A., 2014, Ground-based and UAV-based photogrammetry: A multi-scale, high-resolution mapping tool for structural geology and paleoseismology: Journal of Structural Geology, v. 69, p. 163–178, https://doi.org/10.1016/j.jsg.2014.10.007.

Bemis, S.P., Weldon, R.J., and Carver, G.A., 2015, Slip partitioning along a continuously curved fault: Quaternary geologic controls on Denali fault system slip partitioning, growth of the Alaska Range, and the tectonics of south-central Alaska: Lithosphere, v. 7, p. 235–246, https://doi.org/10.1130/L352.1.

Benowitz, J.A., Layer, P.W., Armstrong, P., Perry, S.E., Haeussler, P.J., Fitzgerald, P.G., and VanLaningham, S., 2011, Spatial variations in focused exhumation along a continental-scale strike-slip fault: The Denali fault of the eastern Alaska Range: Geosphere, v. 7, p. 455–467, https://doi.org/10.1130/GES00589.1.

Binnie, S.A., Phillips, W.M., Summerfield, M.A., Fifield, L.K., and Spotila, J.A., 2010, Tectonic and climatic controls of denudation rates in active orogens: The San Bernardino Mountains, California: Geomorphology, v. 118, p. 249–261, https://doi.org/10.1016/j.geomorph.2010.01.005.

Blisniuk, K., Rockwell, T., Owen, L.A., Oskin, M., Lippincott, C., Caffee, M.W., and Dortch, J., 2010, Late Quaternary slip rate gradient defined using high-resolution topography and ^{10}Be

dating of offset landforms on the southern San Jacinto Fault zone, California: Journal of Geophysical Research, v. 115, B08401, https://doi.org/10.1029/2009JB006346.

Burkett, C.A., Bemis, S.P., and Benowitz, J.A., 2016, Along-fault migration of the Mount McKinley restraining bend of the Denali fault defined by late Quaternary fault patterns and seismicity, Denali National Park & Preserve, Alaska: Tectonophysics, v. 693, p. 489–506, https://doi.org/10.1016/j.tecto.2016.05.009.

Buscher, J.T., and Spotila, J.A., 2007, Near-field response to transpression along the southern San Andreas fault, based on exhumation of the northern San Gabriel Mountains, southern California: Tectonics, v. 26, TC5004, https://doi.org/10.1029/2006TC002017.

Carter, J.N., Luyendyk, B.P., and Terres, R.R., 1987, Neogene clockwise tectonic rotation of the eastern Transverse Ranges, California, suggested by paleomagnetic vectors: Geological Society of America Bulletin, v. 98, p. 199–206, https://doi.org/10.1130/0016-7606(1987)98<199:NCTROT>2.0.CO;2.

Cochran, W., 2016, San Bernardino Mountains, CA 2016 airborne lidar survey: Houston, Texas, National Center for Airborne Laser Mapping (NCALM), distributed by OpenTopography, https://doi.org/10.5069/G9SX6B51.

Cooke, M.L., and Dair, L.C., 2011, Simulating the recent evolution of the southern big bend of the San Andreas fault, Southern California: Journal of Geophysical Research, v. 116, B04405, https://doi.org/10.1029/2010JB007835.

Cowgill, E., Arrowsmith, J.R., Yin, A., Xiaofeng, W., and Zhengle, C., 2004, The Akato Tagh bend along the Altyn Tagh fault, northwest Tibet 2: Active deformation and the importance of transpression and strain hardening within the Altyn Tagh system: Geological Society of America Bulletin, v. 116, p. 1443–1464, https://doi.org/10.1130/B25360.1.

Cunningham, W.D., and Mann, P., 2007, Tectonics of strike-slip restraining and releasing bends, *in* Cunningham, W.D., and Mann, P., eds., Tectonics of Strike-Slip Restraining and Releasing Bends: Geological Society of London Special Publication 290, p. 1–12, https://doi.org/10.1144/SP290.1.

DeMets, C., and Dixon, T.H., 1999, New kinematic models for Pacific–North America motion from 3 Ma to present, I: Evidence for steady motion and biases in the NUVEL-1A model: Geophysical Research Letters, v. 26, p. 1921–1924, https://doi.org/10.1029/1999GL900405.

Dibblee, T.W., Jr., 1961, Evidence of strike-slip movement on northwest-trending faults in Mojave Desert, California, *in* Short Papers in the Geologic and Hydrologic Sciences, Articles 1–146: Geological Survey Research 1961: U.S. Geological Survey Professional Paper 424-B, p. 197–198.

Dibblee, T.W., Jr., 1964a, Geologic map of the Lucerne Valley quadrangle, San Bernardino County, California: U.S. Geological Survey Miscellaneous Geologic Investigations Map I-426, scale 1:62,500, https://doi.org/10.3133/i426.

Dibblee, T.W., Jr., 1964b, Geologic map of the San Gorgonio Mountain quadrangle, San Bernardino and Riverside Counties, California: U.S. Geological Survey Miscellaneous Geologic Investigations Map I-431, scale 1:62,500, https://doi.org/10.3133/i431.

Dibblee, T.W., Jr., 1967a, Geologic map of the Morongo Valley quadrangle, San Bernardino and Riverside Counties, California: U.S. Geological Survey Miscellaneous Geologic Investigations Map I-517, scale 1:62,500, https://doi.org/10.3133/i517.

Dibblee, T.W., Jr., 1967b, Geologic map of the Old Woman Springs quadrangle, San Bernardino County, California: U.S. Geological Survey Miscellaneous Geologic Investigations Map I-518, scale 1:62,500, https://doi.org/10.3133/i518.

Dokka, R.K., and Travis, C.J., 1990a, Late Cenozoic strike-slip faulting in the Mojave Desert, California: Tectonics, v. 9, p. 311–340, https://doi.org/10.1029/TC009i002p00311.

Dokka, R.K., and Travis, C.J., 1990b, Role of the Eastern California shear zone in accommodating Pacific–North American plate motion: Geophysical Research Letters, v. 17, p. 1323–1326, https://doi.org/10.1029/GL017i009p01323.

Fuis, G.S., Scheirer, D.S., Langenheim, V.E., and Kohler, M.D., 2012, A new perspective on the geometry of the San Andreas fault in southern California and its relationship to lithospheric structure: Bulletin of the Seismological Society of America, v. 102, p. 236–251, https://doi.org/10.1785/0120110041.

Glazner, A.F., Walker, J.D., Bartley, J.M., and Fletcher, J.M., 2002, Cenozoic evolution of the Mojave block of southern California, *in* Glazner, A.F., Walker, J.D., and Bartley, J.M., eds., Geologic evolution of the Mojave Desert and southwestern Basin and Range: Geological Society of America Memoir 195, p. 19–41, https://doi.org/10.1130/0-8137-1195-9.19.

Gold, P.O., Behr, W.M., Rood, D., Sharp, W.D., Rockwell, T.K., Kendrick, K., and Salin, A., 2015, Holocene geologic slip rate for the Banning strand of the southern San Andreas Fault, southern California: Journal of Geophysical Research: Solid Earth, v. 120, p. 5639–5663, https://doi.org/10.1002/2015JB012004.

Gomez, F., Nemer, T., Tabet, C., Khawlie, M., Meghraoui, M., and Barazangi, M., 2007, Strain partitioning of active transpression within the Lebanese restraining bend of the Dead Sea Fault (Lebanon and SW Syria), *in* Cunningham, W.D., and Mann, P., eds., Tectonics of Strike-Slip Restraining and Releasing Bends: Geological Society of London Special Publication 290, p. 285–303, https://doi.org/10.1144/290.10.

Harris, R.A., and Day, S.M., 1993, Dynamics of fault interaction: Parallel strike-slip faults: Journal of Geophysical Research, v. 98, p. 4461–4472, https://doi.org/10.1029/92JB02272.

Hauksson, E., Jones, L.M., and Hutton, K., 2002, The 1999 Mw 7.1 Hector Mine, California, earthquake sequence: Complex conjugate strike-slip faulting: Bulletin of the Seismological Society of America, v. 92, p. 1154–1170, https://doi.org/10.1785/0120000920.

Heermance, R.V., and Yule, D., 2017, Holocene slip rates along the San Andreas Fault System in the San Gorgonio Pass and implications for large earthquakes in southern California: Geophysical Research Letters, v. 44, p. 5391–5400, https://doi.org/10.1002/2017GL072612.

Herbert, J.W., Cooke, M.L., Oskin, M., and Difo, O., 2014, How much can off-fault deformation contribute to the slip rate discrepancy within the eastern California shear zone?: Geology, v. 42, p. 71–75, https://doi.org/10.1130/G34738.1.

Jacobs, S.E., 1982, Geology of a part of the upper Santa Ana River Valley, San Bernardino Mountains, San Bernardino County, California [M.S. thesis]: Los Angeles, California State University, 107 p.

Johnson, K., Nissen, E., Saripalli, S., Arrowsmith, J.R., McGarey, P., Scharer, K., Williams, P., and Blisniuk, K., 2014, Rapid mapping of ultrafine fault zone topography with structure from motion: Geosphere, v. 10, p. 969–986, https://doi.org/10.1130/GES01017.1.

Jones, L.E., and Hough, S.E., 1995, Analysis of broadband records from the 28 June 1992 Big Bear earthquake: Evidence of a multiple-event source: Bulletin of the Seismological Society of America, v. 85, p. 688–704.

Kendrick, K.J., Matti, J.C., and Mahan, S.A., 2015, Late Quaternary slip history of the Mill Creek strand of the San Andreas fault in San Gorgonio Pass, southern California: The role of a subsidiary left-lateral fault in strand switching: Geological Society of America Bulletin, v. 127, p. 825–849, https://doi.org/10.1130/B31101.1.

Loveless, J.P., and Meade, B.J., 2011, Stress modulation on the San Andreas fault by interseismic fault system interactions: Geology, v. 39, p. 1035–1038, https://doi.org/10.1130/G32215.1.

Lowe, D.G., 2004, Distinctive image features from scale-invariant keypoints: International Journal of Computer Vision, v. 60, p. 91–110, https://doi.org/10.1023/B:VISI.0000029664.99615.94.

Magistrale, H., and Day, S., 1999, 3D simulations of multi-segment thrust fault rupture: Geophysical Research Letters, v. 26, p. 2093–2096, https://doi.org/10.1029/1999GL900401.

Matti, J.C., and Morton, D.M., 1993, Paleogeographic evolution of the San Andreas fault in southern California: A reconstruction based on a new cross-fault correlation, *in* Powell, R.E., Weldon, R.J., II, and Matti, J.C., eds., The San Andreas Fault System: Displacement, Palinspastic Reconstruction, and Geologic Evolution: Geological Society of America Memoir 178, p. 107–160, https://doi.org/10.1130/MEM178-p107.

McGill, S.F., Owen, L.A., Weldon, R.J., II, and Kendrick, K.J., 2013, Latest Pleistocene and Holocene slip rate for the San Bernardino strand of the San Andreas fault, Plunge Creek, Southern California: Implications for strain partitioning within the southern San Andreas fault system for the last ~35 k.y.: Geological Society of America Bulletin, v. 125, p. 48–72, https://doi.org/10.1130/B30647.1.

McGill, S.F., Spinler, J.C., McGill, J.D., Bennett, R.A., Floyd, M.A., Fryxell, J.E., and Funning, G.J., 2015, Kinematic modeling of fault slip rates using new geodetic velocities from a transect across the Pacific–North America plate boundary through the San Bernardino Mountains, California: Journal of Geophysical Research: Solid Earth, v. 120, p. 2772–2793, https://doi.org/10.1002/2014JB011459.

Meade, B.J., and Hager, B.H., 2005, Block models of crustal motion in southern California constrained by GPS measurements: Journal of Geophysical Research, v. 110, B03403, https://doi.org/10.1029/2004JB003209.

Meisling, K.E., and Weldon, R.J., 1989, Late Cenozoic tectonics of the northwestern San Bernardino Mountains, southern California: Geological Society of America Bulletin, v. 101, p. 106–128, https://doi.org/10.1130/0016-7606(1989)101<0106:LCTOTN>2.3.CO;2.

Miller, F.K., and Cossette, P.M., 2004, Preliminary geologic map of the Big Bear City 7.5′ quadrangle, San Bernardino County, California: U.S. Geological Survey Open-File Report 2004-1193, scale 1:24,000, https://doi.org/10.3133/ofr20041193.

Miller, M.M., Johnson, D.J., Dixon, T.H., and Dokka, R.K., 2001, Refined kinematics of the eastern California shear zone from GPS observations, 1993–1998: Journal of Geophysical

Research, v. 106, p. 2245–2263, https://doi.org/10.1029/2000JB900328.
Molnar, P., and Tapponnier, P., 1977, Relation of the tectonics of eastern China to the India-Eurasia collision: Application of slip-line field theory to large-scale continental tectonics: Geology, v. 5, p. 212–216, https://doi.org/10.1130/0091-7613(1977)5<212:ROTTOE>2.0.CO;2.
Morley, C.K., Smith, M., Carter, A., Charusiri, P., and Chantraprasert, S., 2007, Evolution of deformation styles at a major restraining bend, constraints from cooling histories, Mae Ping fault zone, western Thailand, *in* Cunningham, W.D., and Mann, P., Tectonics of Strike-Slip Restraining and Releasing Bends: Geological Society of London Special Publication 290, p. 325–349, https://doi.org/10.1144/SP290.12.
Morton, D.M., and Matti, J.C., 1993, Extension and contraction within an evolving divergent strike-slip fault complex: The San Andreas and San Jacinto fault zones at their convergence in southern California, *in* Powell, R.E., Weldon, R.J., and Matti, J.C., eds., The San Andreas Fault System: Displacement, Palinspastic Reconstruction, and Geologic Evolution: Geological Society of America Memoir 178, p. 217–230, https://doi.org/10.1130/MEM178-p217.
Onderdonk, N.W., McGill, S.F., and Rockwell, T.K., 2015, Short-term variations in slip rate and size of prehistoric earthquakes during the past 2000 years on the northern San Jacinto fault zone, a major plate-boundary structure in southern California: Lithosphere, v. 7, p. 211–234, https://doi.org/10.1130/L393.1.
Oskin, M., and Iriondo, A., 2004, Large-magnitude transient strain accumulation on the Blackwater fault, Eastern California shear zone: Geology, v. 32, p. 313–316, https://doi.org/10.1130/G20223.1.
Oskin, M., Perg, L., Blumentritt, D., Mukhopadhyay, S., and Iriondo, A., 2007, Slip rate of the Calico fault: Implications for geologic versus geodetic rate discrepancy in the Eastern California Shear Zone: Journal of Geophysical Research, v. 112, B03402, https://doi.org/10.1029/2006JB004451.
Oskin, M., Perg, L., Shelef, E., Strane, M., Gurney, E., Singer, B., and Zhang, X., 2008, Elevated shear zone loading rate during an earthquake cluster in eastern California: Geology, v. 36, p. 507–510, https://doi.org/10.1130/G24814A.1.
Owen, L.A., Finkel, R.C., Minnich, R.A., and Perez, A.E., 2003, Extreme southwestern margin of late Quaternary glaciation in North America: Timing and controls: Geology, v. 31, p. 729–732, https://doi.org/10.1130/G19561.1.
Plattner, C., Malservisi, R., Furlong, K.P., and Govers, R., 2010, Development of the Eastern California Shear Zone—Walker Lane belt: The effects of microplate motion and pre-existing weakness in the Basin and Range: Tectonophysics, v. 485, p. 78–84, https://doi.org/10.1016/j.tecto.2009.11.021.
Rangel, T., and McGill, S., 2016, Low slip rate for San Gorgonio Pass section of the San Andreas fault inferred from geodesy: Geological Society of America Abstracts with Programs, v. 48, no. 4, https://doi.org/10.1130/abs/2016CD-274567.
Reitman, N.G., Bennett, S.E.K., Gold, R.D., Briggs, R.W., and DuRoss, C.B., 2015, High-resolution trench photomosaics from image-based modeling: Workflow and error analysis: Bulletin of the Seismological Society of America, v. 105, p. 2354–2366, https://doi.org/10.1785/0120150041.
Rubin, C.M., 1996, Systematic underestimation of earthquake magnitudes from large intracontinental reverse faults: Historical ruptures break across segment boundaries: Geology, v. 24, p. 989–992, https://doi.org/10.1130/0091-7613(1996)024<0989:SUOEMF>2.3.CO;2.
Schwartz, S.Y., Orange, D.L., and Anderson, R.S., 1990, Complex fault interactions in a restraining bend on the San Andreas Fault, southern Santa Cruz Mountains, California: Geophysical Research Letters, v. 17, p. 1207–1210, https://doi.org/10.1029/GL017i008p01207.
Segall, P., and Pollard, D.D., 1980, Mechanics of discontinuous faults: Journal of Geophysical Research, v. 85, p. 4337–4350, https://doi.org/10.1029/JB085iB08p04337.
Sharp, R.P., Allen, C.R., and Meier, M.F., 1959, Pleistocene glaciers on southern California mountains: American Journal of Science, v. 257, p. 81–94, https://doi.org/10.2475/ajs.257.2.81.
Shelef, E., and Oskin, M., 2010, Deformation processes adjacent to active faults: Examples from eastern California: Journal of Geophysical Research, v. 115, B05308, https://doi.org/10.1029/2009JB006289.
Sieh, K., Jones, L., Hauksson, E., Hudnut, K., Eberhart-Phillips, D., Heaton, T., Hough, S., Hutton, K., Kanamori, H., Lilje, A., Lindvall, S., McGill, S.F., Mori, J., Rubin, C., Spotila, J.A., Stock, J., Thio, H.K., Treiman, J., Wernicke, B., and Zachariasen, J., 1993, Near-field investigations of the Landers earthquake sequence, April to July 1992: Science, v. 260, p. 171–176, https://doi.org/10.1126/science.260.5105.171.
Snavely, N., Seitz, S.M., and Szeliski, R., 2007, Modeling the world from internet photo collections: International Journal of Computer Vision, v. 80, p. 189–210, https://doi.org/10.1007/s11263-007-0107-3.
Spinler, J.C., Bennett, R.A., Anderson, M.L., McGill, S.F., Hreinsdóttir, S., and McCallister, A., 2010, Present-day strain accumulation and slip rates associated with southern San Andreas and eastern California shear zone faults: Journal of Geophysical Research, v. 115, B11407, https://doi.org/10.1029/2010JB007424.
Spotila, J.A., and Anderson, K.B., 2004, Fault interaction at the junction of the Transverse Ranges and Eastern California shear zone: A case study of intersecting faults: Tectonophysics, v. 379, p. 43–60, https://doi.org/10.1016/j.tecto.2003.09.016.
Spotila, J.A., and Sieh, K., 2000, Architecture of transpressional thrust faulting in the San Bernardino Mountains, southern California, from deformation of a deeply weathered surface: Tectonics, v. 19, p. 589–615, https://doi.org/10.1029/1999TC001150.
Spotila, J.A., Farley, K.A., and Sieh, K., 1998, Uplift and erosion of the San Bernardino Mountains associated with transpression along the San Andreas fault, California, as constrained by radiogenic helium thermochronometry: Tectonics, v. 17, p. 360–378, https://doi.org/10.1029/98TC00378.
Spotila, J.A., Farley, K.A., Yule, J.D., and Reiners, P.W., 2001, Near-field transpressive deformation along the San Andreas fault zone in southern California, based on exhumation constrained by (U-Th)/He dating: Journal of Geophysical Research, v. 106, p. 30,909–30,922, https://doi.org/10.1029/2001JB000348.
Sylvester, A.G., 1988, Strike-slip faults: Geological Society of America Bulletin, v. 100, p. 1666–1703, https://doi.org/10.1130/0016-7606(1988)100<1666:SSF>2.3.CO;2.
Tapponnier, P., and Molnar, P., 1976, Slip-line field theory and large-scale continental tectonics: Nature, v. 264, p. 319–324, https://doi.org/10.1038/264319a0.
Thatcher, W., Savage, J.C., and Simpson, R.W., 2016, The Eastern California Shear Zone as the northward extension of the southern San Andreas Fault: Journal of Geophysical Research: Solid Earth, v. 121, p. 2904–2914, https://doi.org/10.1002/2015JB012678.
Ullman, S., 1979, The interpretation of structure from motion: Proceedings of the Royal Society B: Biological Sciences, v. 203, p. 405–426, https://doi.org/10.1098/rspb.1979.0006.
U.S. Geological Survey and California Geological Survey, 2006, Quaternary fault and fold database for the United States: http://earthquake.usgs.gov/hazards/qfaults/ (accessed October 2017).
Wakabayashi, J., 2007, Stepovers that migrate with respect to affected deposits: Field characteristics and speculation on some details of their evolution, *in* Cunningham, W.D., and Mann, P., eds., Tectonics of Strike-Slip Restraining and Releasing Bends: Geological Society of London Special Publication 290, p. 169–188, https://doi.org/10.1144/SP290.4.
Wald, D.J., and Heaton, T.H., 1994, Spatial and temporal distribution of slip for the 1992 Landers, California, earthquake: Bulletin of the Seismological Society of America, v. 84, p. 668–691.
Weldon, R.J., II, and Sieh, K.E., 1985, Holocene rate of slip and tentative recurrence interval for large earthquakes on the San Andreas fault, Cajon Pass, southern California: Geological Society of America Bulletin, v. 96, p. 793–812, https://doi.org/10.1130/0016-7606(1985)96<793:HROSAT>2.0.CO;2.
Wells, D.L., and Coppersmith, K.J., 1994, New empirical relationships among magnitude, rupture length, rupture width, rupture area, and surface displacement: Bulletin of the Seismological Society of America, v. 84, p. 974–1002.
Wesnousky, S.G., 1988, Seismological and structural evolution of strike-slip faults: Nature, v. 335, p. 340–343, https://doi.org/10.1038/335340a0.
Westoby, M.J., Brasington, J., Glasser, N.F., Hambrey, M.J., and Reynolds, J.M., 2012, 'Structure-from-Motion' photogrammetry: A low-cost, effective tool for geoscience applications: Geomorphology, v. 179, p. 300–314, https://doi.org/10.1016/j.geomorph.2012.08.021.
Yeats, R.S., Sieh, K.E., and Allen, C.R., 1997, The Geology of Earthquakes: New York, Oxford University Press, 576 p.
Yule, D., 2009, The enigmatic San Gorgonio Pass: Geology, v. 37, p. 191–192, https://doi.org/10.1130/focus022009.1.
Yule, D., and Sieh, K., 2003, Complexities of the San Andreas fault near San Gorgonio Pass: Implications for large earthquakes: Journal of Geophysical Research, v. 108, 2548, https://doi.org/10.1029/2001JB000451.